ADDIS ABABA UNIVERSITY

ADDIS ABABA INSTITUTE OF TECHNOLOGY

SCHOOL OF CIVIL AND ENVIRONMENTAL ENGINEERING

Multi-scale Simulation of Time-Dependent Deformation Behavior of Reinforced Concrete Bridge Decks with 3-Dimensional Material-Structure Coupled Analysis

A Thesis in Structural Engineering

By Erkeno Yohannes Sido

February 2020

Addis Ababa

A Thesis

Submitted in Partial Fulfillment of the Requirements for the Degree of Master of Science

ADDIS ABABA UNIVERSITY
ADDIS ABABA INSTITUTE OF TECHNOLOGY
SCHOOL OF CIVIL AND ENVIRONMENTAL ENGINEERING

The undersigned have examined the thesis entitled '**Multi-scale Simulation of Time-Dependent Deformation Behavior of Reinforced Concrete Bridge Decks with 3-Dimensional Material-Structure Coupled Analysis**' presented by **Erkeno Yohannes Sido**, a candidate for the degree of **Master of Science** and hereby certify that it is worthy of acceptance.

Approved by Board of Examiners

Dr. Esayas Gebreyouhannes		
Advisor	Signature	Date
Dr. Abraham Gebre		
Internal Examiner	Signature	Date
Dr. Bedilu Habte		
External Examiner	Signature	Date
Dr. Mebruk Mohammed		
School Dean	Signature	Date

UNDERTAKING

I certify that research work titled “Multi-scale Simulation of Time-Dependent Deformation Behavior of Reinforced Concrete Bridge Decks with 3-Dimensional Material-Structure Coupled Analysis” is my own work. The work has not been presented elsewhere for assessment. Where material has been used from other sources, it has been properly referred.

_____

Erkeno Yohannes Sido

ABSTRACT

A concrete structure subjected to a load deform in both immediate and with time. Time-dependent deformations are caused by the coupled effect of sustained stress and stress due to environmental conditions (temperature and relative humidity). The effects of these actions are a basic creep, drying creep and shrinkage. In this research, the time-dependent deformation behavior of the T-girder bridge deck due to the coupled effect of sustained truckload and environmental conditions was investigated by material-structure coupled analysis.

A full 3-dimensional T-girder deck was modeled, discretized and analyzed in finite element package DuCOM-COM3 for material-structure coupled analysis. The standard truckload, annual average ambient temperature and relative humidity of Addis Ababa and Semera were used for this study.

The results of this study indicated that temperature and relative humidity significantly affect the strength and deformation properties of the concrete. For the mix design of the compressive strength of 30MPa, incorporating the effect of temperature and humidity, the compressive strength of 42MPa was attained at the environmental condition of Addis Ababa with an annual average temperature of 23.5°C and relative humidity of 64.2%. For the same mix, the strength reduces to 30MPa at the environmental condition of Semera with an annual average temperature of 34.3°C and relative humidity of 47.7%. Deformation of interlayer pores and incomplete hydration due to moisture migration at an early age was observed as the cause for the strength reduction and increase in deflection of girder in the long term. It was observed that with the effect of ambient temperature and relative humidity, the increase in mid-span deflection up to 4 times as large as the value due to only sustained load without the effect of environmental conditions.

The results have shown that the deformation of interlayer pores at an early age crack was found significant for the larger size. The reduction in strength properties of the girder deck up to 14% was observed when compared to the cube specimen at a temperature of 34.3°C and relative humidity of 47.7%.

Keywords: Multi-scale modeling, Time-dependent deformation, Creep, Shrinkage, Environmental conditions, Moisture migration, DuCOM-COM3, Material-structure coupled analysis.

ACKNOWLEDGMENTS

I sincerely express my profound gratitude to Dr. Esayas Gebreyouhannes, my advisor, for his guidance, encouragement, and suggestions and constructive advice throughout the course of the thesis. He provided me DuCOM-COM3 software that he has developed with his colleagues at the University of Tokyo and trained and guided me on how to use it. I come away with a sense of accomplishment and pride in what he has helped me to achieve. It was an honor and privilege for me to conduct the research with him.

Finally, I would like to thank my Professors in the institute who shared knowledge and made me capable to accomplish this study. I would also like to thank my family members and friends for their invaluable support.

TABLE OF CONTENTS

LIST OF TABLES

LIST OF FIGURES

LIST OF SYMBOLS AND ABBREVIATIONS

FE	Finite Element
RC	Reinforced Concrete
$A_{c,eff}$	The cross-sectional area of concrete in tension surrounding reinforcement
A_s	Total tension reinforcement area
ε_t	The total strain
ε_i	Instantaneous strain
ε_c	Creep strain
ε_v	Volumetric strain
ε_e	Elastic strain
ε_{sh}	Shrinkage strain
ε_T	Thermal strain
ε_d	Delayed elastic strain
ε_f	Flow strain
∞	Infinity
DL	Dead load
P	Truckload
E	Elastic modulus of concrete
E_a	Elastic modulus of aggregate
ψ	The ratio of fine aggregate to the total aggregate of the concrete
E_0	Elastic modulus of concrete at the time of loading
f_c	Cylindrical compressive strength of concrete
f_{ck}	Characteristic compressive strength of concrete

μ	Poisson's ratio of concrete
μ_a	Poisson's ratio of aggregate
υ	Creep coefficient
h	Height of cross-section
d	Distance from extreme compression fiber to centroid of a tension bar
x	Neutral axis depth
b_w	Width of the cross-section
ACI	American concrete institute
C2S	Belite (calcium silicates)
C3S	Alite (calcium silicates)
C4AF	Calcium ferrite
C3A	Calcium aluminate
C-S-H	Calcium silicate hydrates
Ca (OH)2	Calcium hydroxide
J	Joule
CS2H	Calcium silicate hydrates (gypsum)

CHAPTER 1 INTRODUCTION

1.1 General Background of the Study

1.1.1 Time-dependent deformation

A concrete structure subjected to a load exhibits both instantaneous and time-dependent deformation. When a sustained load is applied, the deformation of the structure gradually increases and could be many times as large as its initial value. This gradual development of strain is caused by basic creep, drying creep and shrinkage.

The inelastic and time-dependent strains due to creep and shrinkage results in the decks:

- To increase in deformation
- To loss prestress
- To redistribute stresses and internal actions and result in deformation and cracks.

In order to make the structure serviceable in its intended life, accurate and reliable predictions of both immediate and time-dependent deformation of concrete structures are important. Creep and shrinkage are often responsible for excessive deflection at service load. For the structure restrained, the shrinkage may cause crack propagation with the time that could result in serviceability and durability failures after the long-term.

Unless the time-dependent deformations are accounted for properly in the design, the serviceability failures of bridge decks that comply with code requirements could be in excessive deflection due to creep and shrinkage. The reason is that the serviceability provisions in the design codes are empirical and may not often realistically account for the effects of creep and shrinkage of the concrete. Prediction for serviceability is complicated by the non-linear and inelastic behavior of concrete due to creep and shrinkage at service load in high ambient temperature and low humid environment.

Creep refers to a sustained load-induced deformation at a constant stress while shrinkage is stress-independent phenomena due to environmental conditions. In high temperature and low humid environment, drying shrinkage is the most significant and caused by a

decrease in relative humidity of interlayer pores which leads to an increase in capillary tension of pore water.

To effectively predict the time-dependent deformation behavior of concrete structures, reliable input parameters for creep and shrinkage characteristics and analysis platform that can include the effect of ambient temperature and relative humidity are necessary.

In this study, a coupled material-structure integrated analysis that includes the effect of material properties, ambient temperature and humidity on creep and shrinkage was investigated. To identify the effect of these parameters, this research gives the insight to predict the time-dependent deformation and cracking of concrete bridge deck in-service conditions.

This research focuses on the combined effect of both immediate and time-dependent creep and shrinkage induced deformation.

1.2 Statement of the Problem

Creep and shrinkage are unavoidable phenomena and affect concrete material long-term properties. If not accurately accounted for in the design stage, the concrete structure could be in excessive long-term deflection and crack. The existing bridge condition assessment should be monitored on excessive deflection and cracking. To know when to maintain, prediction of time-dependent effect is required. In addition to deflection and crack, predicting the progression of creep and shrinkage used to know the critical time for prestressing loss in bridge decks.

1.3 Objective

1.3.1 General Objective

The main objective of this thesis is to investigate the time-dependent deformation behavior of reinforced concrete bridge decks due to the combined effect of sustained load and environmental conditions.

1.3.2 Specific Objective

- To investigate the effect of ambient temperature and relative humidity on the strength properties of concrete
- To investigate the effect of early-age strength properties on the long-term deflection
- To investigate the combined effect of sustained service truckload and environmental conditions (relative humidity and ambient temperature) on long term deflection of the bridge deck.
- To predict the long-term deformation of a 20m span T-girder bridge and compare its deflection with the deflection value considered during design.

1.4 Scope of the Study

This study only focusses on the time-dependent deformation of a 20m span T-girder bridge deck due to fixed-point standard truckload and environmental conditions of Addis Ababa and Semera. The research doesn't cover the effect of moving load on a time-dependent deflection. The time-dependent deformation behavior in this study accounts for the mutual effect of both material and geometric nonlinearity.

1.5 Methodology

The research work was carried out at different phases. In the first stage, the relevant literature review on the time-dependent deformation was done. In the second stage, collecting design data of the bridge deck, material mix proportion, and environmental conditions (temperature and relative humidity). In the last phase of the study, multiscale simulation by material-structure coupled analysis using nonlinear finite element software was conducted. The nonlinear finite element analysis tool DuCOM-COM3 was used.

1.6 Significance of the study

This study is significant for the design sector, that the effect of creep and shrinkage play a major role in reducing the serviceability and durability of concrete structures by increasing

the deformation behavior of bridge decks and hence accurately and efficiently accounted. The study is significant for the construction sector that creep and shrinkage have a significant effect on prestress loss and relaxation of prestressed concrete, thus to be considered during construction

1.7 Report Organization

The thesis report is made up of five chapters. Chapter 1 introduces the general background, problem statement, objectives, and scope of this research. Chapter 2 presents a literature review related to the research. This chapter reports a review of the research works on the time-dependent deformation behavior of concrete structures, creep and shrinkage, constitutive concrete models for time-dependent analysis, existing creep and shrinkage code models. Chapter 3 discusses on T-girder deck modeling and analysis in DuCOM-COM3 software. In this chapter, the material and the girder deck are modeled, discretized and analyzed in the software based on a constitutive model accounting for time-dependent deformation analysis. Chapter 4 reports analysis results and discussions. In this chapter analysis results of different parameters are reported in tables and figures and brief discussions are performed. Chapter 5 reports the conclusions and recommendations drawn from the study and a discussion of future research requirements.

CHAPTER 2 LITERATURE REVIEW

2.1 Time-dependent deformation of bridge decks

Concrete bridge deck undergoes time-dependent deformations during the application of internal and/or external stresses. Time-dependent deformation in the concrete deck is a progressive and permanent deformation under constant load. In the study by (Pauw, 1971), it has been shown that long term deformation due to time-dependent parameters is the result of a gradual reduction in stiffness of the structures. Bridges decks undergo excessive deflection and crack in the long term due to creep and shrinkage. These factors affect the service life of bridges. Time-dependent deformation of concrete creep and shrinkage results in stress redistribution, which triggers damage and cracking. According to (ACI 209,2008), mechanisms responsible for time-dependent deformation are:

- Redistribution of capillary water or interlayer water movement
- Sliding or shearing of gel particles lubricated by adsorbed water (viscous flow strain)
- Sliding or shearing movement of the crystalline lattice (plastic flow strain)
- Permanent plastic deformation caused by microcracking.

The research by (Bažant et al., 2009), has shown that Creep and shrinkage have been a pervasive cause of damage and excessive deflection in structures. The case study result of (Bažant et al., 2009) on a bridge with a span of 241m was 1.24m more than the predicted value after 20 years. This excessive deflection is due to failure to account for the effect of creep and shrinkage. The conclusion of this study is that if the time-dependent deformation effect is not appropriately considered in the design phase of concrete structures, the structure may suffer from excessive deflection due to creep and shrinkage with time.

Creep and shrinkage are non-separable phenomena of one to other. That is shrinkage in concrete structures facilitates the total creep in concrete (Gilbert et al., 2010) and (Pauw, 1971).

2.2 Time-dependent material properties

2.2.1 Creep in concrete

Creep deformation depends on applied load, ambient temperature, relative humidity, porosity and degree of hydration. When porosity increases the stress will be concentrated in the load-bearing skeleton and thus increases the creep formation (Wittmann, 2009). Creep in concrete is the effect of the viscoelastic deformation of the micropores due to applied stress (ACI 231,2010). Creep is an increase in a strain under a coupled effect of sustained load and stress due to environmental conditions. The stress due to the combined effect of external load and internal stress can be several times larger than the strain due to only sustained load (Neville, 1996).

The effect of creep increases with time but in decreasing rate (Gilbert et al., 2010). About 50 percent of the final creep of its intended life generally taken as 100 years will occur within 2-3 months and more than 90 percent of the final creep will occur after 2-3 years (Gilbert et al., 2010).

Although the progression of creep is unlimited with time, long-time creep and shrinkage test results on concrete have shown that there is a small increase in creep after 30 years (Neville, 1996).

2.2.2 Mechanism of creep formation in concrete

Creep in the hardened cement paste is due to the deformation of a solid cement gel with capillary interlayer pores. The cement gel is a colloidal sheet of calcium silicate hydrates separated by spaces containing absorbed water (Gilbert et al., 2010). According to (Neville, 1996) mechanisms for creep formation are:

- sliding of the colloidal sheets in the cement gel between the layers of absorbed water
- expulsion and decomposition of the interlayer water within the cement gel
- elastic deformation of the aggregate and the gel crystals as viscous flow and seepage occur within the cement gel
- local fracture within the cement gel involving the breakdown and formation of physical bonds
- mechanical deformation and plastic flow.

Creep response depends on the packaging density distribution of calcium-silicate-hydrates (C-S-H). At high-stress levels, additional deformation occurs due to the stress concentration on the skeleton, there will be deformation of the bond between the cement paste and aggregate particles (Vandamme & Ulm, 2009).

Figure 2-1 from test results, showed that the upper and lower limit of creep of concrete with time (Neville, 1996). As shown in Figure 2-1, more than 50% of 20 years creep was occur in 3 months and more than 80% happened after 2 years of loading. Even though it was not significant, there was creep after 20 years. Based on the figure, the study indicated that if creep after 1 year under load is taken as unity, then the average values of creep at later ages are:

1.14 times of 1 year creep is nearly the same as 2 years creep

1.20 times of 1 year creep is nearly the same as 5 years creep

1.26 times of 1 year creep is nearly the same as 10 years creep

1.33 times of 1 year creep is nearly the same as 2 years creep

1.36 times of 1 year creep is nearly the same as 30 years creep.

For design purposes, it was recommended to apply a 30 years creep as an ultimate creep (Neville, 1996).

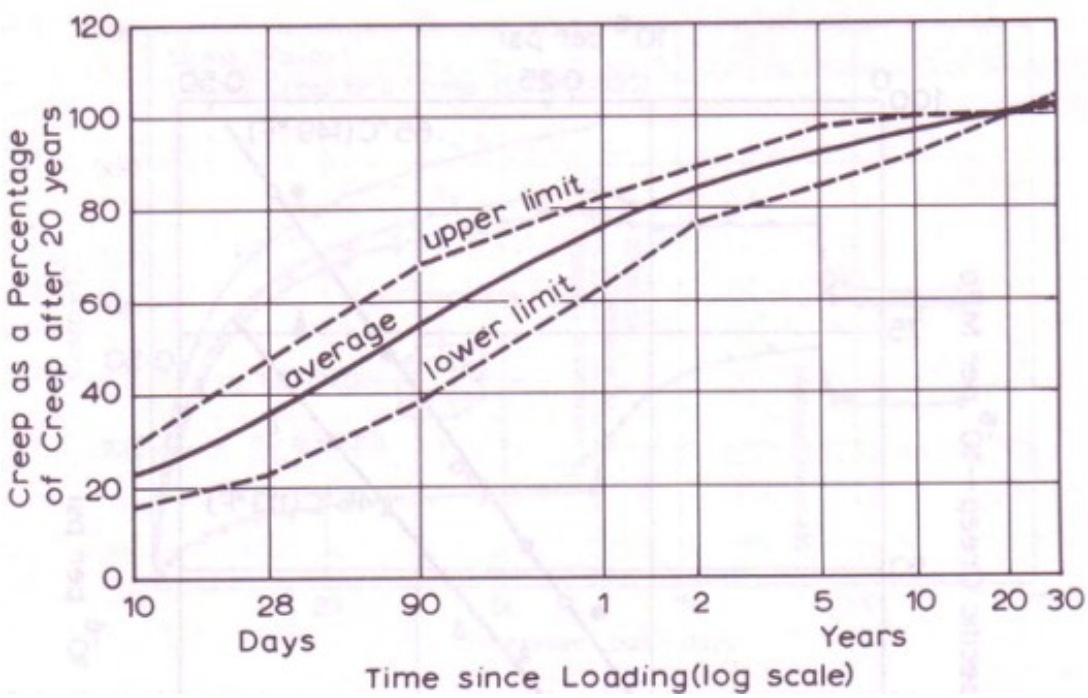

Figure 2-1: Range of creep-time curves for different concretes at various RH (Neville, 1996)

2.2.3 Shrinkage in concrete

Shrinkage is the time-dependent strain at a constant temperature without any external stress. Early-age deformation and cracking are due to autogenous shrinkage and drying shrinkage. Autogenous shrinkage is thermal deformation due to cement hydration whereas drying shrinkage is a reduction in volume when the concrete members are exposed to the environment. During the chemical process of hydration of cement, chemical shrinkage creates the underlying deriving force for the occurrence of autogenous shrinkage. Autogenous shrinkage is the macroscopic bulk deformation of the cementitious material system not subjected to an external system (ACI 231,2010) and (ACI 209,2008).

In the drying process, as thick elements lose water slowly, the dimensions of the structural elements have a great influence on the shrinkage strain. Shrinkage starts after the capillary water has evaporated and gel water is lost due to drying flow in gel water.

The investigation by (Wittmann, 2009) showed that the process of shrinkage formation is that initially the capillary shrinkage follows the evolution of the capillary pressure but after few hours capillary pressure collapses and capillary shrinkage approaches a final value. At this moment the cementitious system in the mix becomes unstable and the remaining water

moves into the spaces between the particles (Figure 2-2). As it has shown in Figure 2-2, capillary pressure increases with time and it is a major mechanism for the shrinkage of hardened concrete. By wetting the concrete surface, the equilibrium with capillary pressure can be maintained and the formation of delayed wide cracks can be avoided (Wittmann, 2009).

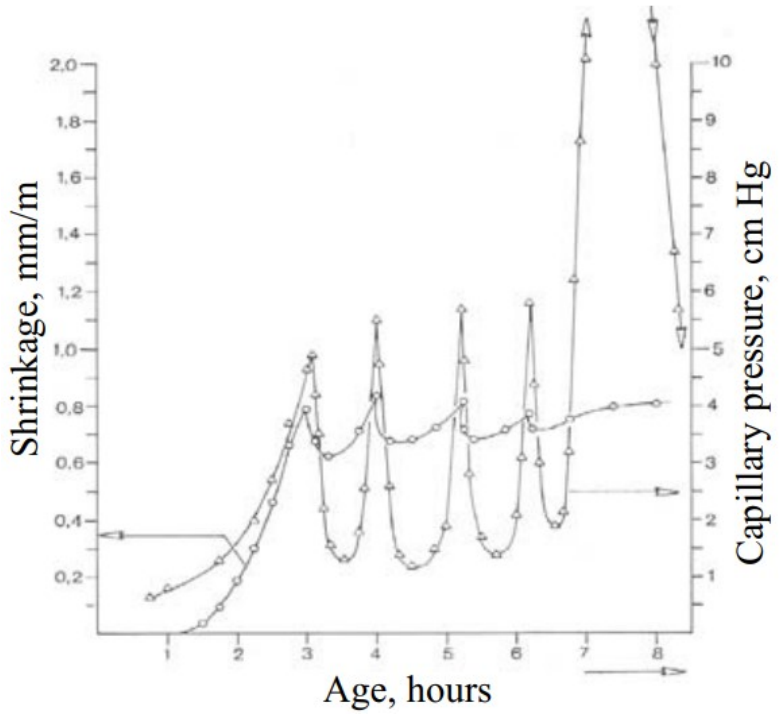

Figure 2-2: Evolution of capillary pressure and capillary shrinkage in young concrete during drying and rewetting (Wittmann, 2009)

Similar to creep, there are different factors that affect creep. As discussed in different works of literature, factors that affect creep also affect the shrinkage property of concrete.

2.2.4 Factors influencing creep and shrinkage

Numerous researches have presented several factors that influence creep and shrinkage properties of concrete. The most important factors that influence creep and shrinkages are modulus of elasticity of aggregate, the porosity of aggregates, the strength of concrete, properties of cement, ambient relative humidity and temperature (Neville, 1996) and (Rüsch et al., 1983).

The work of (Baweja, 2001) showed that the variation of creep and shrinkage properties in concrete are affected by internal factors, composition, and quality of concrete and aggregate size while the humidity and temperature are external ambient factors.

2.2.4.1 Modulus of elasticity of aggregate

Aggregate type affects the response of the structure for creep and shrinkage. Based on the investigation result of (Neville, 1996) and (Tanaka & Hashida, 2009), the modulus of elasticity of aggregate is the most important factor that influences creep and shrinkage. A significant difference between creep strains of concretes made with different aggregate types on constant humidity was noted (Rüsch et al., 1983). As shown in Figure 2-3, the aggregates in the decreasing order of creep formation are sandstone; basalt; gravel; granite; quartz and limestone (Neville, 1996). The results of Figure 2-3 indicated that the amount of creep in 20 years with concrete made up of sandstone is more than double when compared to the creep value of concrete with limestone.

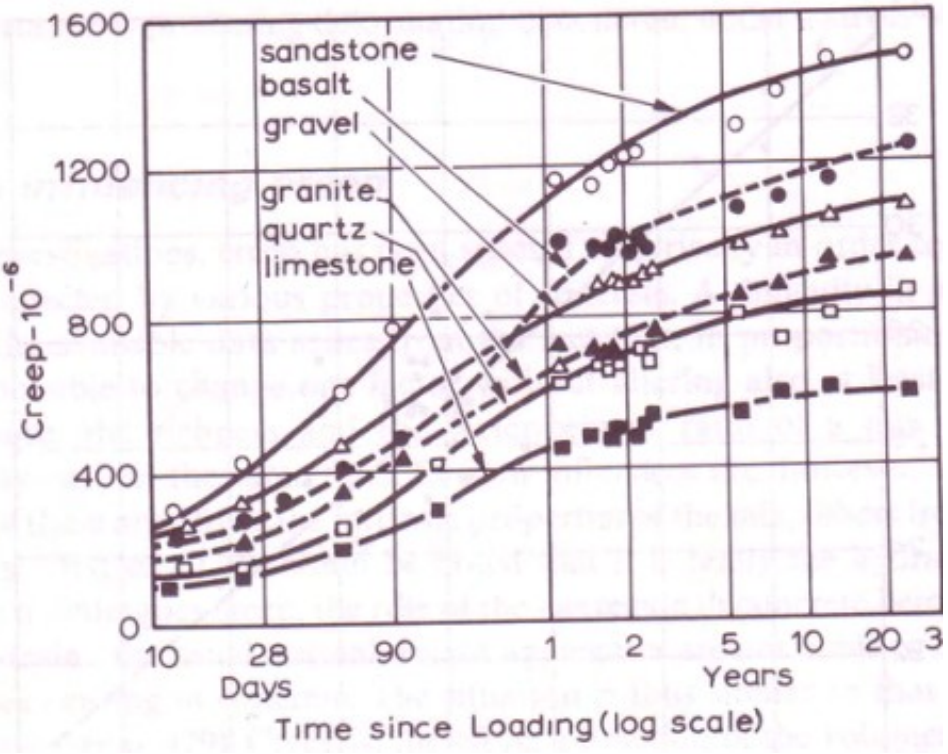

Figure 2-3: Creep of concretes of fixed proportions but with different aggregates loaded at the age of 28 days, and stored at the air with a temperature of 21 $°C$ and relative humidity of 50 percent (Neville, 1996)

2.2.4.2 Environmental exposure conditions

The exposure conditions are the ambient temperature, relative humidity and the ratio of volume to drying surface (v/s) of concrete.

2.2.4.3 Sensitivity to ambient temperature

Creep and shrinkage strains increase with temperature since the deformability of the hydrated cement gel increases and drying is accelerated when the temperature increases. According to the study by (Maekawa et al., 2003), it was indicated that as the temperature rises, its influence on creep and shrinkage increases. The research showed that for concrete protected against drying at temperatures of 0°C to 20°C, creep hardly depends on temperature drying, whereas when the temperature rises from 20°C to 100°C the increase in creep is by a factor of 2 to 3 (Maekawa et al., 2003). It has been shown that when concrete is allowed to dry at the higher temperature, there occurs a drying flow; but later the flow rate drops significantly since dry concrete flows very little. Therefore, the effect of temperature on creep and shrinkage cannot be neglected. The mean temperature of 0°C hardly changes creep and shrinkage characteristics with respect to 20°C, but a mean temperature of 40°C increases creep effect by about 25 %, on average.

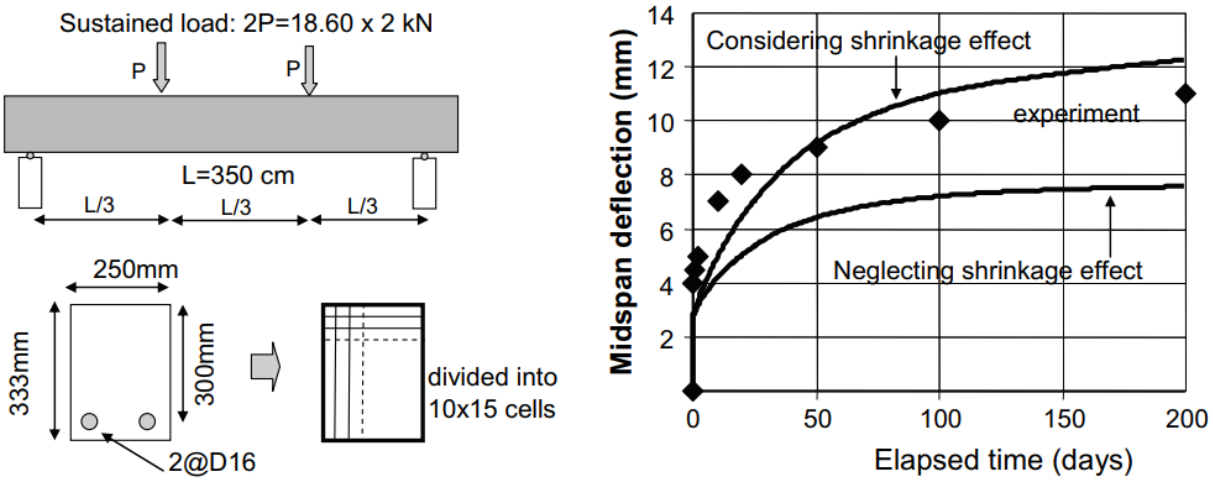

Figure 2-4: The effect of shrinkage on deflection properties of concrete (Maekawa et al., 2003)

2.2.4.4 Sensitivity to relative humidity

One of the most external factors influencing creep is the relative humidity of the air surrounding the concrete. Creep increases as the ambient temperature are high and the relative humidity low (Neville, 1996) and (Rüsch et al., 1983). From Figure 2-5, it can be

noted that creep increases with time and when relative humidity decreases. 20 years creep at 100% relative humidity is about half of the creep at 70%.

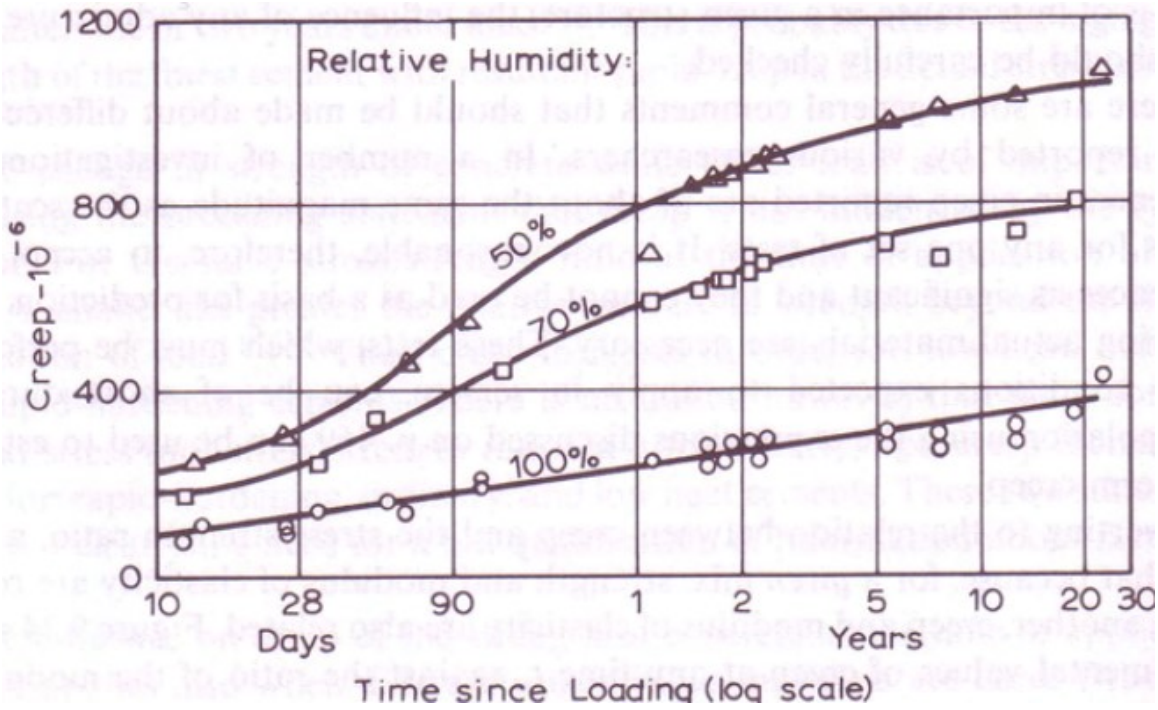

Figure 2-5: Creep of concrete cured in the fog for 28 days, then loaded and stored at a different relative humidity (Neville, 1996)

The study by (Rüsch et al., 1983) presented in Figure 2-6 showed the influence of humidity on shrinkage. The 10,000 days shrinkage strain at 70% RH is more than 90% of the shrinkage strain at 100% RH.

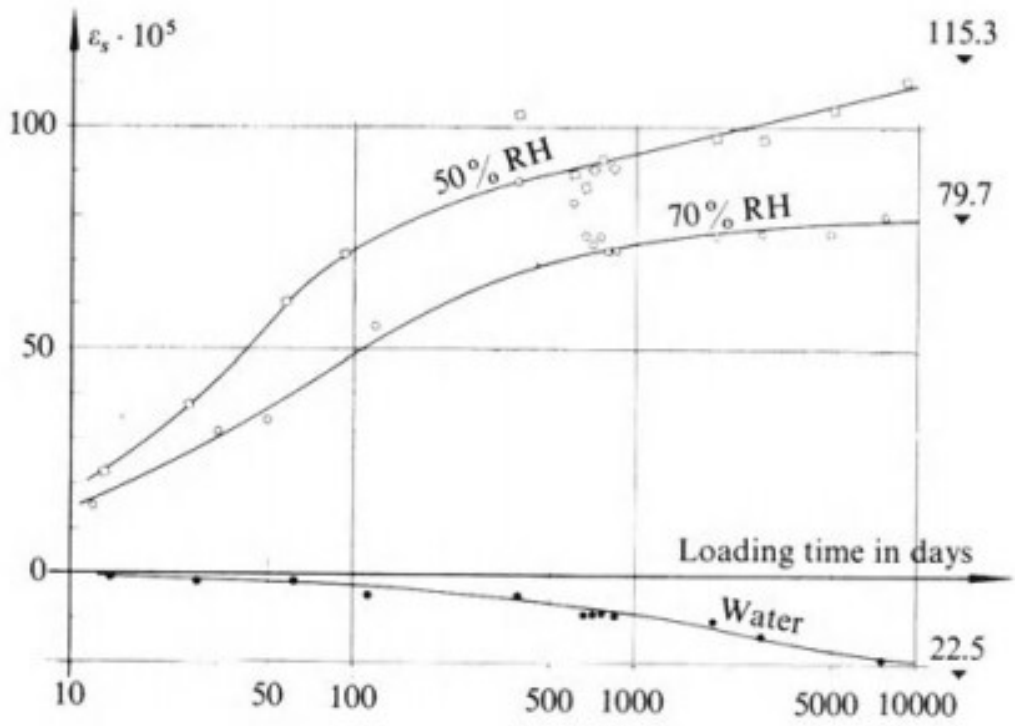

Figure 2-6: Effect of relative humidity on the shrinkage of concrete (Rüsch et al., 1983)

2.2.4.5 Strength of concrete

The strength property of concrete has a significant effect on creep and shrinkage. Creep progression is inversely proportional to the strength of concrete at the time of load application (Neville, 1996).

The research of (Gilbert et al., 2010) has shown that the creep properties of concrete decrease as the concrete strength increases which is in a good agreement with an investigation by (Neville, 1996). It was noted that creep in higher-strength concrete is less than that in lower-strength concrete. Creep also decreases as the water-to-cement ratio is reduced (Gilbert et al., 2010).

It has been shown in the research of (Neville, 1996) that creep of concrete, the volumetric content of aggregate, and volumetric content of un hydrated cement are related by:

$$\log\frac{c_p}{c} = \alpha \log\left(\frac{1}{(1-g-u)}\right) \quad \text{Eq 2-1}$$

Where:

c = creep of concrete

g = volumetric content of aggregate

u = volumetric content of unhydrated cement

$$\alpha = \frac{3(1-\mu)}{1+\mu+2(1-2\mu_a)\frac{E}{E_a}} \qquad \text{Eq 2-2}$$

c_p = the creep of neat cement paste of the same quality as used in concrete;

μ_a =Poisson's ratio of aggregate;

μ =the Poisson's ratio of concrete;

E = the modulus of elasticity of concrete;

E_a = the modulus of elasticity of aggregate.

From the expression, it can be noted that higher the modulus of aggregate, the greater the restraint offered by the aggregate against creep that decreases the creep rate. It was also pointed out that increasing the aggregate content by 65 to 75 percent in volume will decrease the creep effect by 10 percent (Neville, 1996).

2.2.4.6 Porosity

The total porosity and pores size distribution depend on water to cement ratio and degree of hydration (Wittmann, 2009). In this study, it was pointed out that the drying process and shrinkage of porous material are governed by pore size distribution.

Due to increasing stress concentrations on the load-bearing solid skeleton as porosity increases, it has a strong influence on creep formation. The porosity of aggregate has also been found to influence the creep of concrete because the aggregate with higher porosity generally has a lower modulus of elasticity.

Concrete raw materials and mix proportions are also parameters that affect creep and shrinkage (Mu et al., 2009). Properties of cement have also a significant influence on creep. The fineness of cement affects the strength development at early ages and thus

influences creep (Neville, 1996). Creep of concrete made with expansive cement is larger than when only Portland cement is included in the mix and water-reducing and set-retarding admixtures increase the basic creep (Neville, 1996). When Portland cement reacts with water, some of the heat is liberated while the concrete is young and easily deformable and undergo a characteristic volume change with about 7% gross volume decrease (Wittmann, 2009).

2.2.5 Influence of creep and shrinkage on deformation

A comparative simulation study by (Y.Qiang&T.Teng, 2014) has shown the effect of creep and shrinkage on the deflection of bridge decks. The results presented in this study (Figure 2-7) have shown that about140mm mid-span deflection without the effect of creep and shrinkage. As can be seen from Figure 2-8 by including the effect of creep and shrinkage, the mid-span deflection increases to 210mm which is about a 50% increase in deflection. The finding of this study showed that the effect of creep and shrinkage of concrete must be taken into account in bridge design and neglecting these parameters may lead to unrealistic long-term deflection.

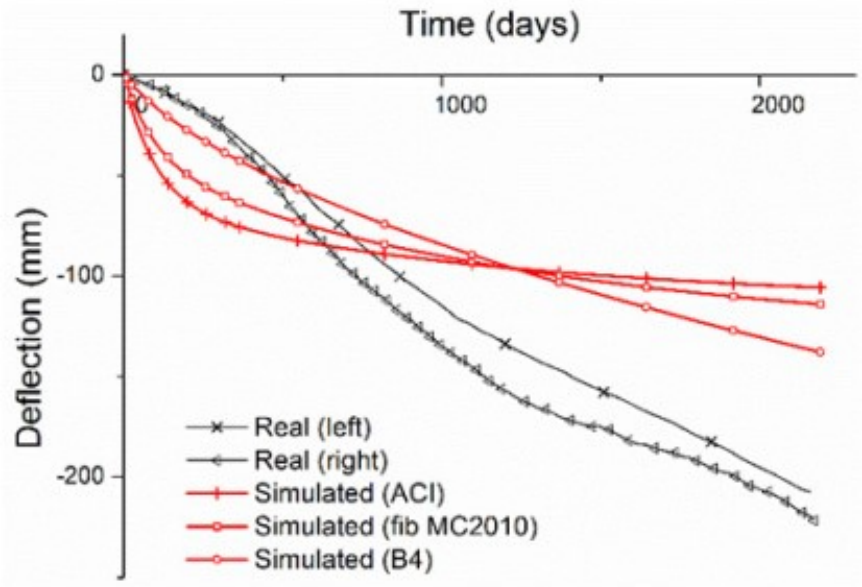

Figure 2-7: Deflection at mid-span at 7 years without including creep effect(Y.Qiang&T.Teng,2014)

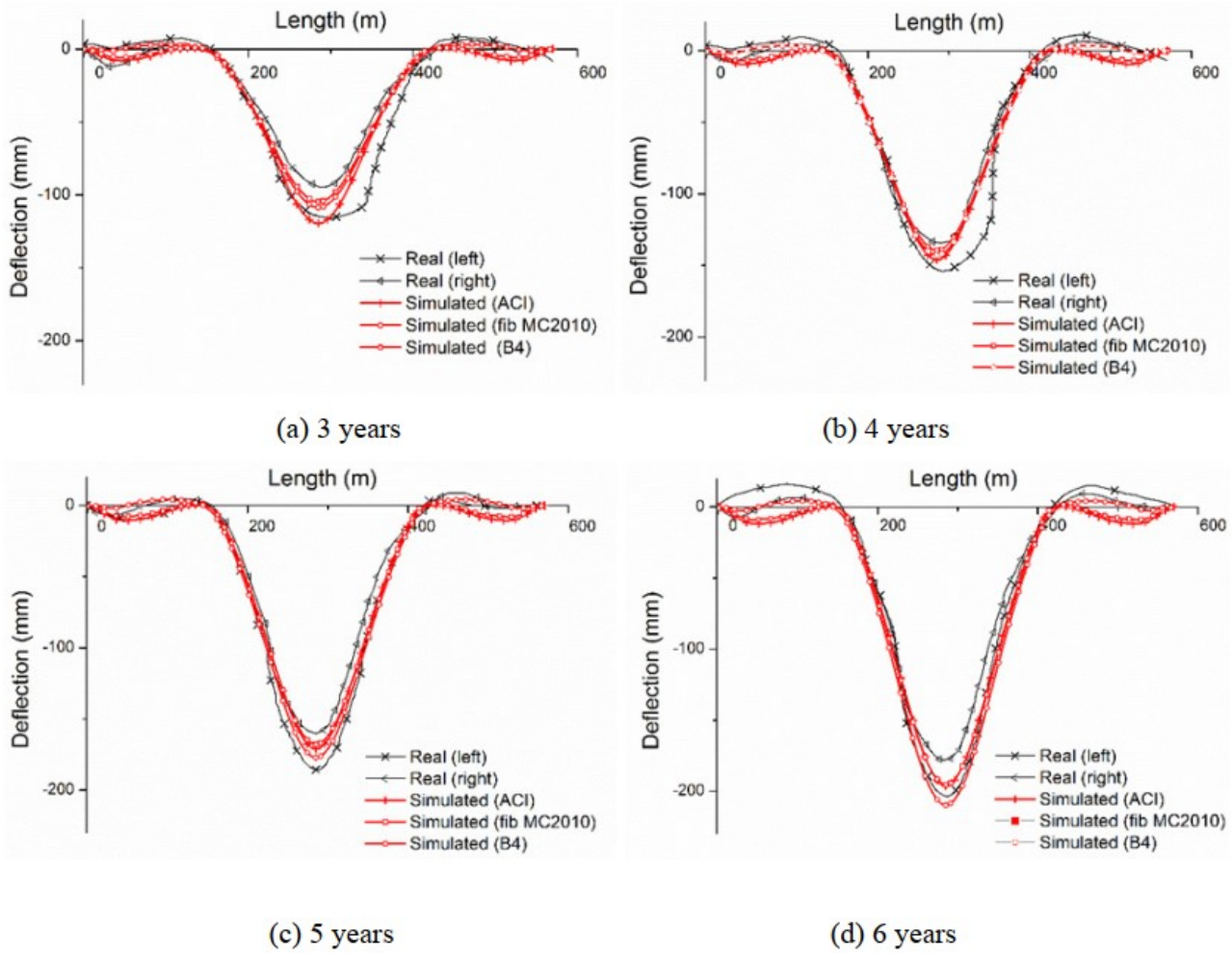

Figure 2-8: Deflection at mid-span at 6 years by including creep (Y.Qiang&T.Teng, 2014)

2.3 Components of strain in concrete structures

Various researches have investigated different components of strain in concrete structures under sustained load. According to (Pauw, 1971), the total strain in concrete structures is resulting from the instantaneous response, the time-dependent strains caused by creep and the time-dependent strains caused by volume changes due to changes in the hygro-thermal state and physio-chemical changes such as shrinkage and swelling.

$$\varepsilon_t = \varepsilon_i + \varepsilon_c + \varepsilon_v \qquad \text{Eq 2-3}$$

Where:

ε_t = the total strains;

ε_i = the strains resulting from instantaneous response to loading both recoverable (elastic) and irrecoverable (plastic);

ε_c = the time-dependent strains caused by creep for a given stress history and under given hydro-thermal conditions;

ε_v = the time-dependent strains caused by volume changes due to changes in the hygro-thermal state and physio-chemical changes such as shrinkage and swelling due to moisture changes, thermal expansion or contraction and chemical expansion or contraction. As presented in (Pauw, 1971) and (Min et al., 2009) the greater portion of total deformation in concrete structures is deformation due to drying creep and shrinkage in concrete.

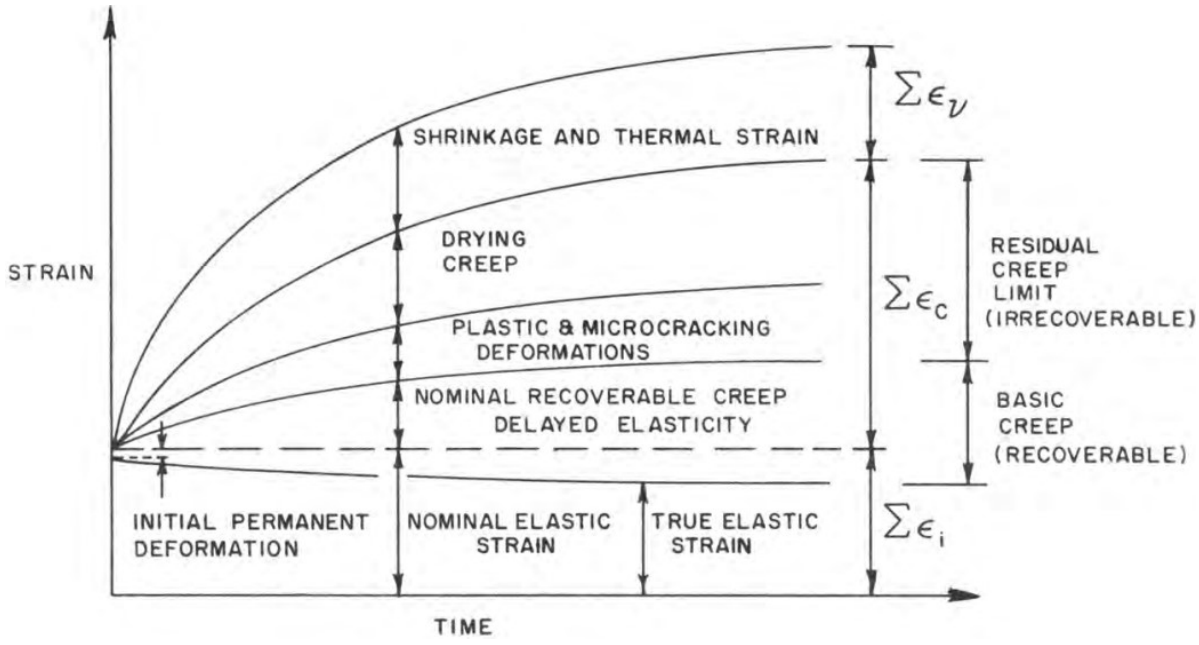

Figure 2-9: Strains in a loaded concrete specimen in a drying environment (Pauw, 1971)

The total deformation in concrete is due to basic creep, drying creep and shrinkage (Min et al., 2009). In this study, it was also shown that creep and shrinkage effects are non-separable phenomena.

$$\varepsilon(t) = \varepsilon_e(t) + \varepsilon_c(t) + \varepsilon_{sh}(t) + \varepsilon_T(t) \quad \text{Eq 2-4}$$

Where:

$\varepsilon(t)$ = the strain of concrete

$\varepsilon_e(t)$ = elastic strain

$\varepsilon_c(t)$ = creep strain

$\varepsilon_{sh}(t)$ = shrinkage strain

$\varepsilon_T(t)$ =thermal strain

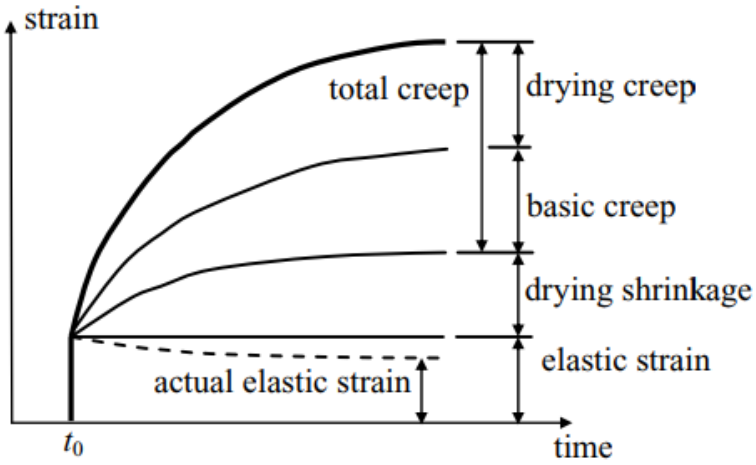

Figure 2-10: Deformation of concrete for sustained load and drying circumstance (Min et al., 2009)

In the study by (Pauw, 1971), it is noted that the over-all time-dependent increase in deformation due to creep and shrinkage are dependent phenomena to which the principle of superposition can be applied. A similar conclusion was pointed in (Gilbert et al., 2010) in a way that creep and shrinkage are non-separable and each other are dependent phenomena. Thus, creep is significantly greater when accompanied by shrinkage. The research study of (Mu et al., 2009) investigated that the shrinkage and creep of concrete are intrinsically linked and any factor influencing the shrinkage of concrete will also affect the creep behavior. According to (Mu et al., 2009), a high shrinkage concrete will generally have high creep and a low shrinkage concrete will usually exhibit low creep. Creep is normally considered as time-dependent deformation in excess of shrinkage (Neville,

1996). The time-dependent deformation components are elastic strain, shrinkage strain, and strains due to basic and drying creeps (Figure 2-11).

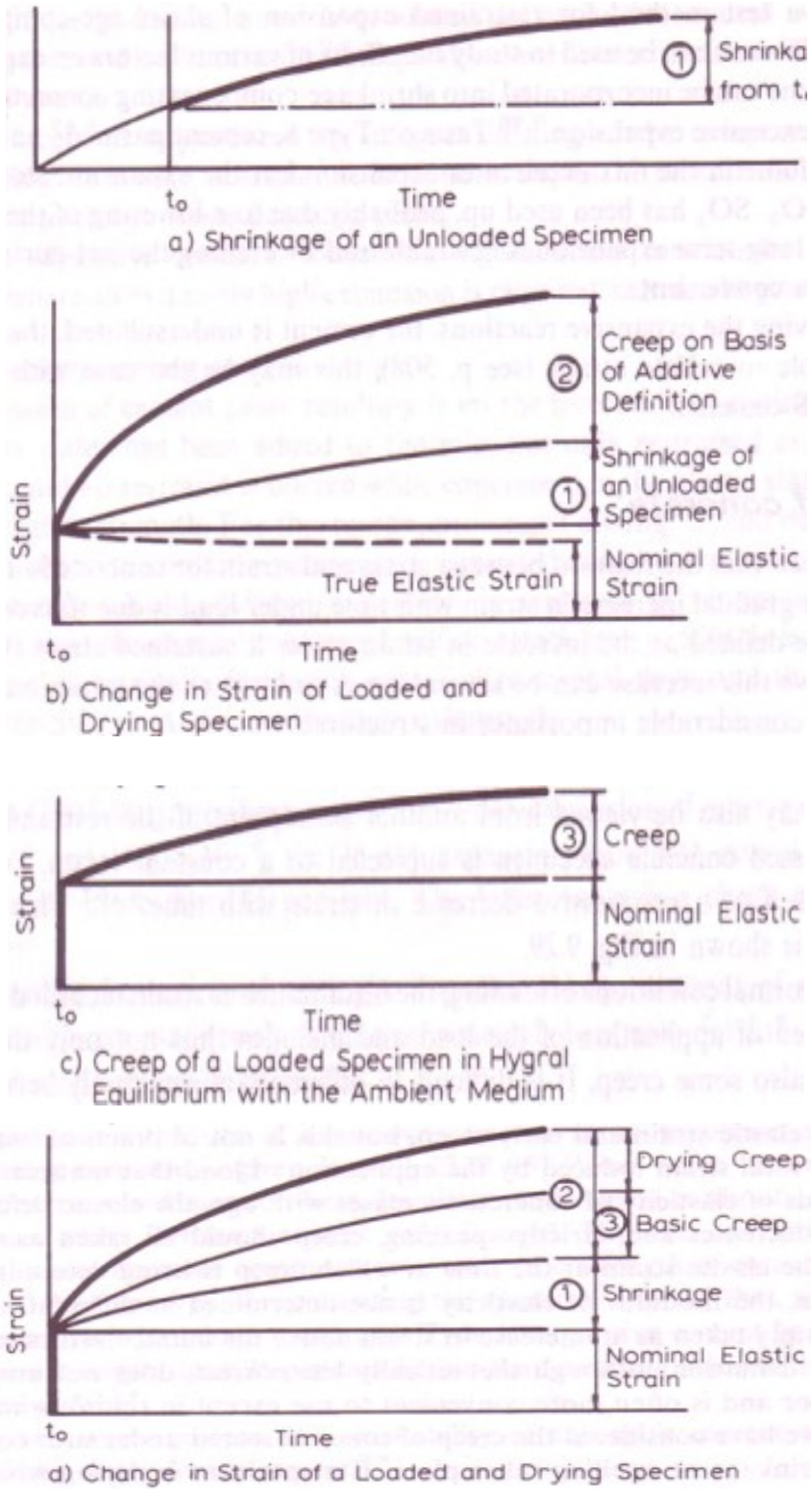

Figure 2-11: Time-dependent deformations in concrete (Neville, 1996)

In concrete material, in which the viscous hydrated cement paste interacts with elastic aggregates and the delayed elasticity reaches a level of about 40% of the instantaneous elastic strain (Rüsch et al., 1983). The components of strain under this study are treated by separating creep strain into two.

Creep under sustained load = delayed elastic deformation + flow

$$\varepsilon_c = \varepsilon_d + \varepsilon_f \qquad \text{Eq 2-5}$$

$$\varepsilon_c = \varepsilon_d + \varepsilon_i + \bar{\varepsilon_f}. \qquad \text{Eq 2-6}$$

Where:

ε_c = creep under sustained load

ε_d = delayed elastic strain (basic creep strain)

ε_i = rapid initial strain (instantaneous strain)

$\bar{\varepsilon_f}$ = remaining flow

creep= delayed elastic strain + rapid initial strain + remaining flow

A similar finding was presented in the study by (Pauw, 1971) and summarized the strain component as time-dependent (drying creep and shrinkage) and load-dependent (basic creep) (Figure 2-12).

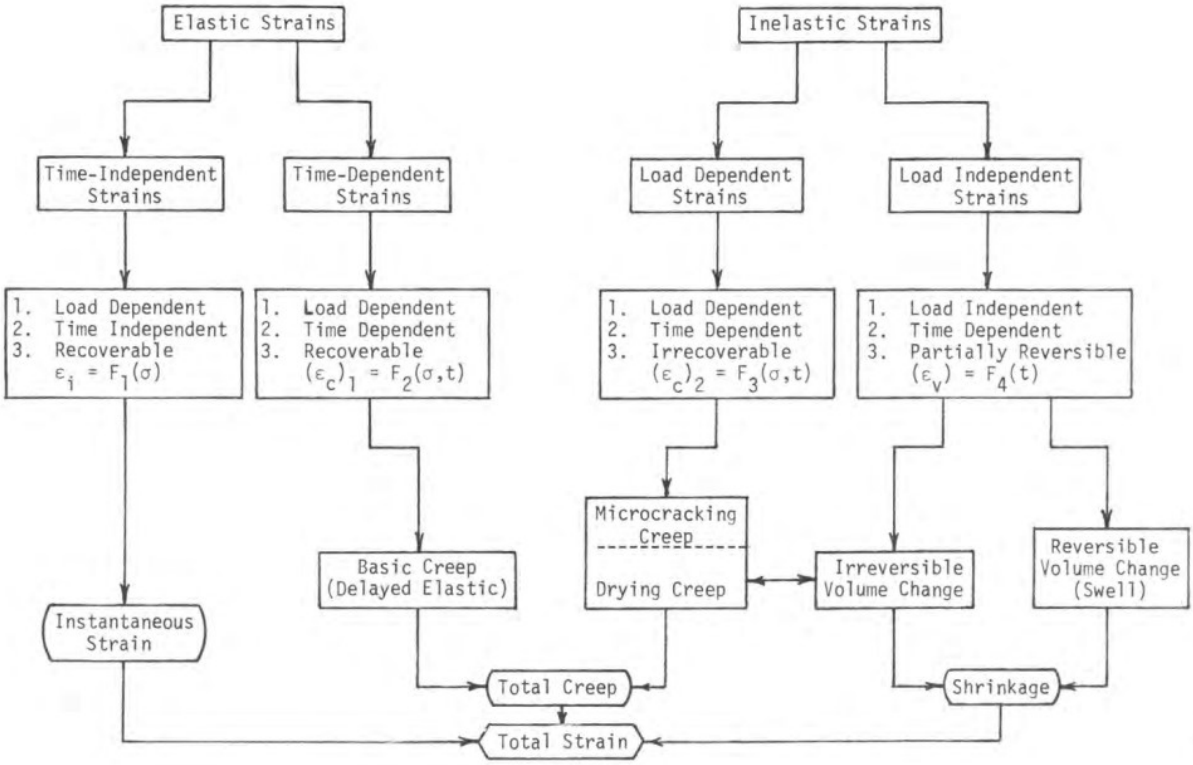

Figure 2-12: Strain Components (Pauw, 1971)

The research by (Rüsch et al., 1983) summarized a similar finding as (Pauw, 1971) on the components of strain due to creep and shrinkage (Figure 2-13). In this study, the total strain is the coupled effect of elastic strain, flow and shrinkage strain.

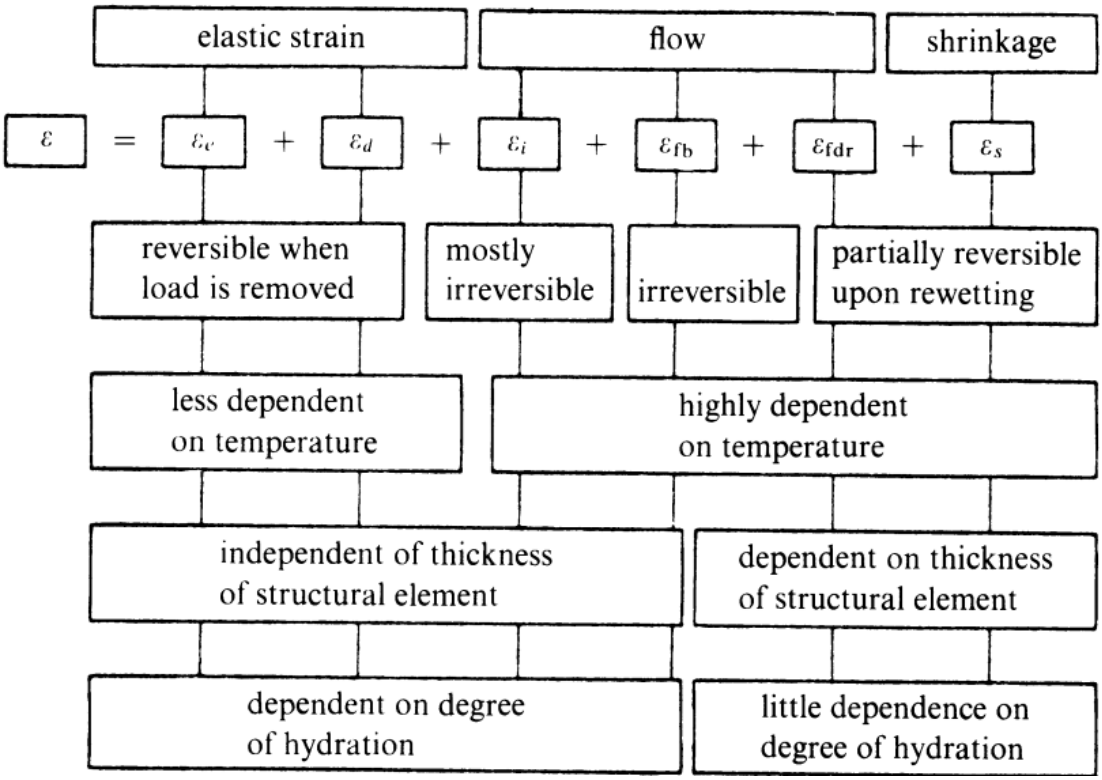

Figure 2-13: Components of creep strain in concrete (Rüsch et al., 1983)

2.4 Deformation process in cement paste

The early age deformation process in cement paste is due to the removal of water from the paste. According to the cement paste model in (Asamoto et al., 2006), moisture migration has a significant effect on the deformation of micropores at an early age. Based on Figure 2-14, it can be pointed that instantaneous stiffness loss results in elastic strain, removal of capillary water results in viscoelastic strain, whereas the removal of gel water and interlayer water result in viscoplastic and plastic strains respectively.

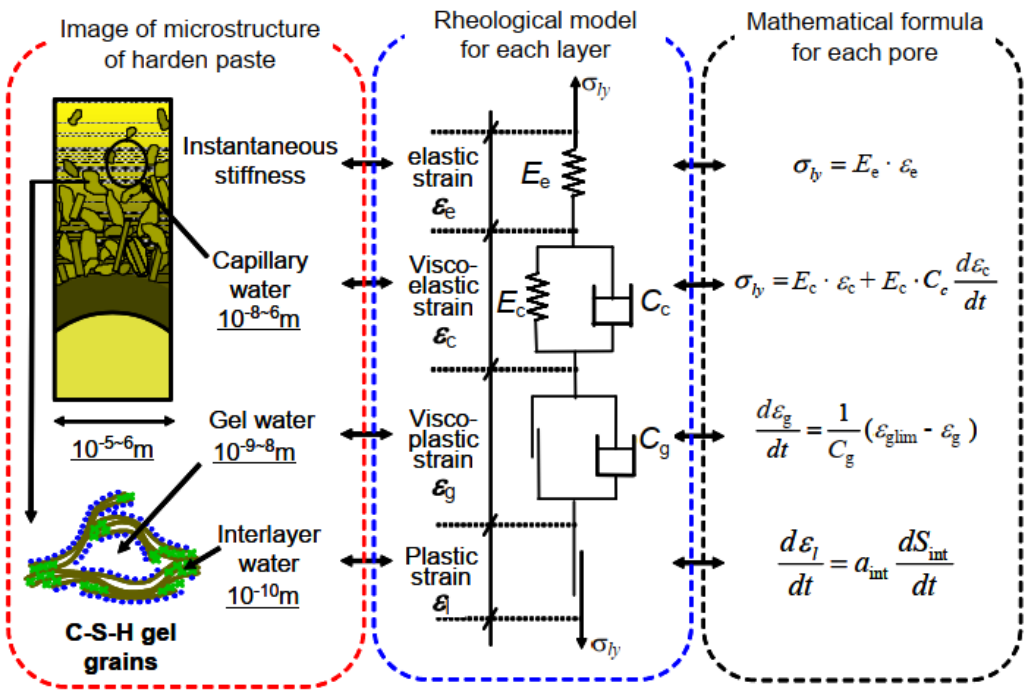

Figure 2-14: Rheological model for each layer of cement paste (Asamoto et al., 2006)

2.5 Multi-scale Constitutive Model of Concrete

The time-dependent constitutive model of concrete for creep and shrinkage prediction is presented and different verifications were made in the study by (Asamoto et al., 2006) and (Maekawa et al., 2003).

In a multiscale constitutive model, concrete is idealized in a way as a two-phase composite in which cement paste and elastic aggregate coexist (Ishida et al., 2018). In this model, the aggregate is assumed to be rigid and behave elastic deformation, and induce shrinkage stress in the paste.

The hardened cement paste matrix is considered to be an assembly of finite fictitious clusters and as cement hydration proceeds the number of the clusters increases. The overall capacity of the cement paste is obtained by the integral of each cluster to which the time-dependent constitutive modeling of C-S-H hydrate is applied. Based on the amount of water present in the micro-pores, the time-dependent deformation consisting of elastic strain due to instantaneous stiffness, viscoelastic strain due to capillary water, plastic strain due to interlayer water and visco-plastic strain due to gel water are computed. According to (Maekawa et al., 2003) and (Asamoto et al., 2006), the force of capillary pressure in the

model is computed in accordance with moisture state as a mechanism of driving force for volume change and when the equilibrium between shrinkage stresses and externally applied stresses is satisfied.

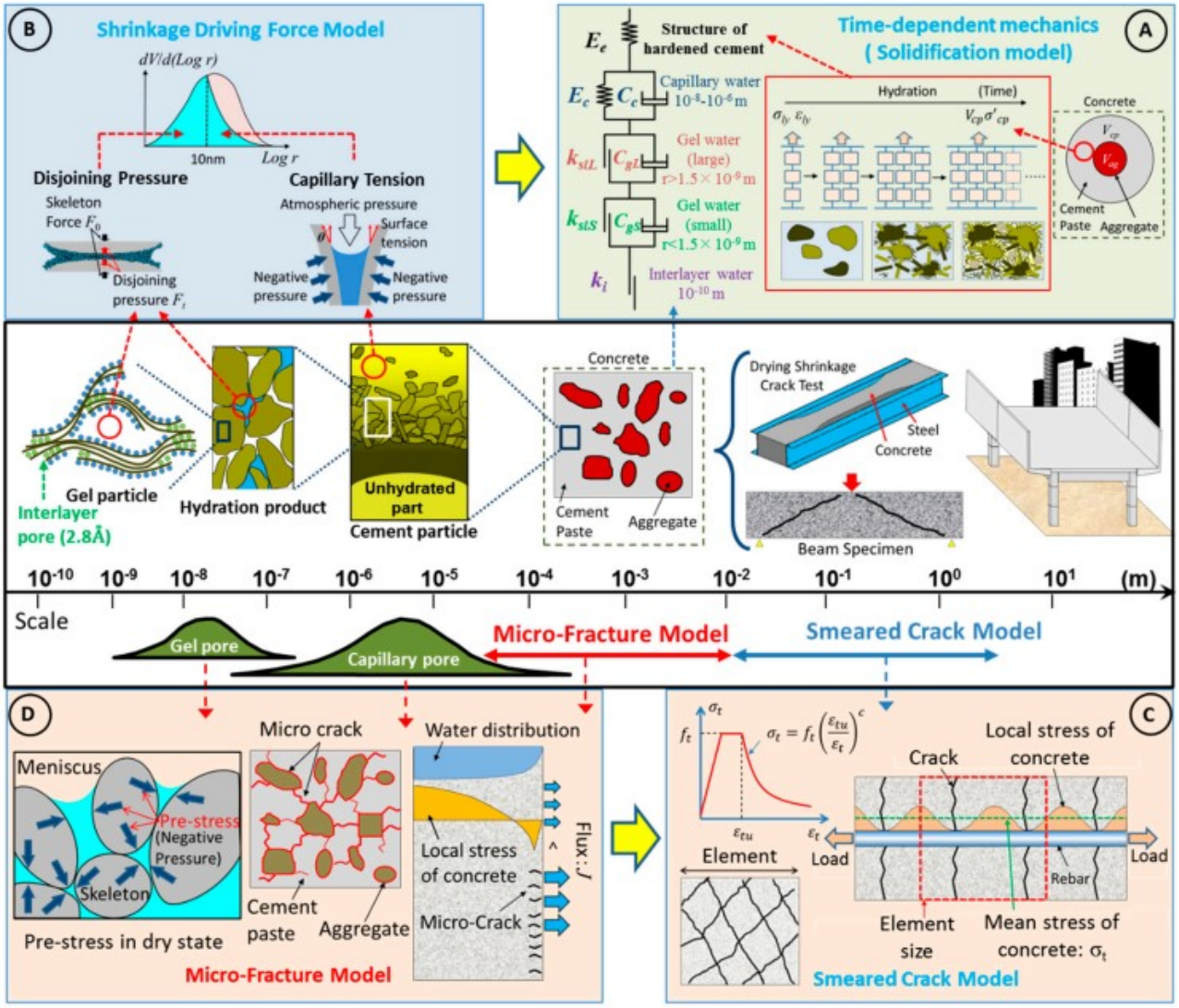

Figure 2-15: Multiscale and multi-physical modeling to simulate time-dependent deformation and cracking (Ishida et al., 2018) and (Maekawa et al., 2003)

When the water in the micro-pores is lost during the drying process, a water meniscus will form in microscale pores and some shrinkage stresses are generated by capillary tension. Whereas in the nanoscale pores, shrinkage stresses are generated by disjoining pressure (Bažant & Milan, 2018).

2.6 Modeling in DuCOM-COM3

The model in Figure 2-15 is the multi-scale and multi-physical model implemented in the software to simulate time-dependent deformation and cracking behavior of concrete structures. The model consists of thermodynamic multi-chemo-physical modeling with DuCOM platform and nonlinear structural analysis with COM3 part. DuCOM platform includes multicomponent hydration, micropore structure formation, moisture migration, and equilibrium while the COM3 platform is a 3-dimensional finite element analysis that implements constitutive laws of uncracked and cracked and hardening or matured concrete (Maekawa et al., 2003).

The basic input data for DuCOM-COM3 are mix proportions, structural geometry, and boundary conditions in terms of environmental exposure of the structure over the time-space domain, the kinematic chemo-physical and mechanical events on elements would be solved at the same time step for both material and structure (Ishida et al., 2018). Time-dependent properties of concrete, elastic modulus, temperature, pore pressure, creep, moisture status, total porosity of the interlayer, gel and capillary pores are computed internally based on material micromodels inside the DuCOM platform (Maekawa et al., 2003). The software integrates the actual phenomena of Figure 2-16.

The two primary factors triggering to time-dependent deformations are mechanically induced stress due to applied load and thermodynamically induced internal stresses due to environmental conditions (temperature and humidity) in time.

(Maekawa et al., 2011) has shown a summary of the material-structure analysis link phenomenon implemented in the DuCOM-COM3. According to the outline, the DuCOM platform is a thermodynamic analytical system where hydration, microstructure formation and mass transport occur. On the other hand, the COM3 platform is a nonlinear structural analytical system where plastic deformation, damage and cracks occur. The linked analysis enables to simulate the time-dependent deformation from the hardening stage to the deterioration stage.

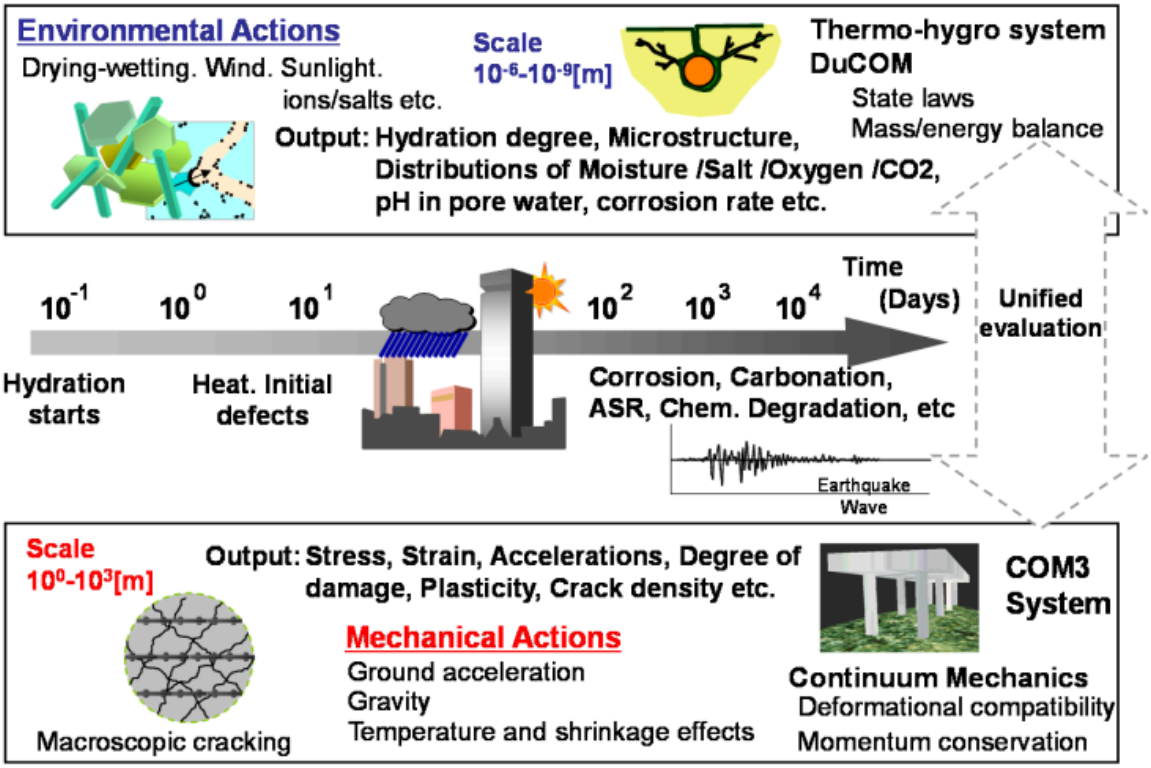

Figure 2-16: Multiscale and multi-physical modeling to simulate time-dependent concrete performance (Ishida et al., 2018) and (Maekawa et al., 2003)

Plastic localization of reinforcement and averaging of local stress and strain along the reinforcement is important for rationally simulating largely deformed elements.

The local stress and strain in steel and concrete are modeled. Tension softening and stiffening was introduced in the software to model actual behavior (Maekawa et al., 2003). The instantaneous evolution of a tension fracture as given in the paper by the formula:

$$H = -(1+\alpha)\left(\frac{f_t}{E_o}\right)\varepsilon_{cr}^{\alpha}.\varepsilon_{\max}^{-(\alpha+2)}, \text{when } d_\varepsilon > 0 \text{ and } \varepsilon = \varepsilon_{\max} \qquad \text{Eq 2-7}$$

$$H = 0, \text{when } d_\varepsilon \le 0 \text{ and } \varepsilon < \varepsilon_{\max} \qquad \text{Eq 2-8}$$

Where: H = represents the envelope of the tension stress-strain curve after cracking

α = represents tension stiffening associated with bonding for RC and tension softening associated with crack localized inside for plain concrete.

ε_{cr} is the crack strain defined equal to $\frac{2f_t}{E_o}$ and $\varepsilon_{\max}$ is the updated maximum value of tensile strain ε in the past history. Derivative H characterizes the envelope of the tension stress-strain curve after cracking. This formula covers the tension stiffness of RC associated with bonding (α =0.4).

E_o is the non-dimensional initial stiffness of concrete solid. It has a peak strain value of $E_o = 2.0$ as stated in the study by (Maekawa et al., 2003).

f_t is uniaxial tensile strength.

The authors recommended the value of α =0.4 for RC to consider tension stiffening whereas α =2 for plain concrete to consider the tension softening.

2.7 Exothermic hydration process of cement

Portland cement consists of pulverized cement clinker and gypsum. There are four major minerals in the clinker. Alite mainly C_3S, belite mainly C_2S, aluminate mainly C_3A and ferrite mainly C_4AF. C_3S and C_2S are calcium silicates comprising about 85% of the cement clinker. C_4AF and C_3A are minerals to occupy the space when cement clinker. As reported in (Maekawa et al., 2003), the process of hydration is a complex process since the rate of hydration and the type of hydrates vary significantly among clinker minerals. In the hydration process, C_3S and C_2S produce both calcium silicate hydrates (C-S-H) and calcium hydroxide (Ca $(OH)_2$). But C_3A and C_4AF produce ettringite effect with gypsum (CS2H). In this process, calcium aluminate sulfates are produced when the gypsum is reacted and ettringite will be converted into a mono sulfate. All of these processes occur simultaneously in the hardening cement paste and generate heat. From total generated heat, C_3S generates 504 J/g, C_2S generates 260 J/g, C_3A generates 870 J/g, and C_4AF generates 420 J/g. This shows that more heat is produced by C_3A and C_3S (Maekawa et al., 2003). The model of this phenomenon developed to represent the reaction is shown below in Figure 2-17 (Maekawa et al., 2003). The reaction rates are thus, in the order of C_3A> C_3S> C_4AF> C_2S. It has been shown that as the amount of C_3A and C_3S increases in the cement, the early age strength of the cement paste will increase.

This implies the mineral reactions affect each other. These interactions can be considered through variables like temperature, free water remaining in the concrete and degree of hydration. It was presented in (Maekawa et al., 2003) that the amount of water required for the cement to fully hydrate is about 40% of the cement's weight and that some cement remains un hydrated if the water to cement ratio is less than 40%.

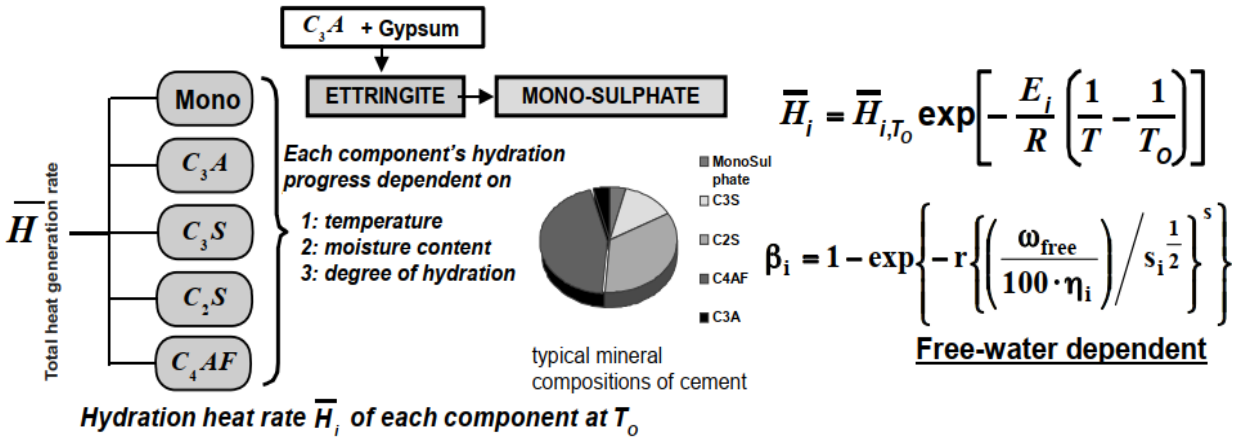

Figure 2-17: Multi-mineral component model of cement hydration and heat generation (Maekawa et al., 2003)

It is showed in the study by (Neville, 1996) when the content of C_3S increases in the cement, heat generation also increases and thus the strength of concrete increases and has a significant effect on time-dependent behavior of concrete (Figure 2-18).

From Figure 2-19, the research work has shown that the effect of C_3S and C_2S in the cement is to increase strength development. Moreover, it clearly shows that the early age strength increases as the content of C_3S increases.

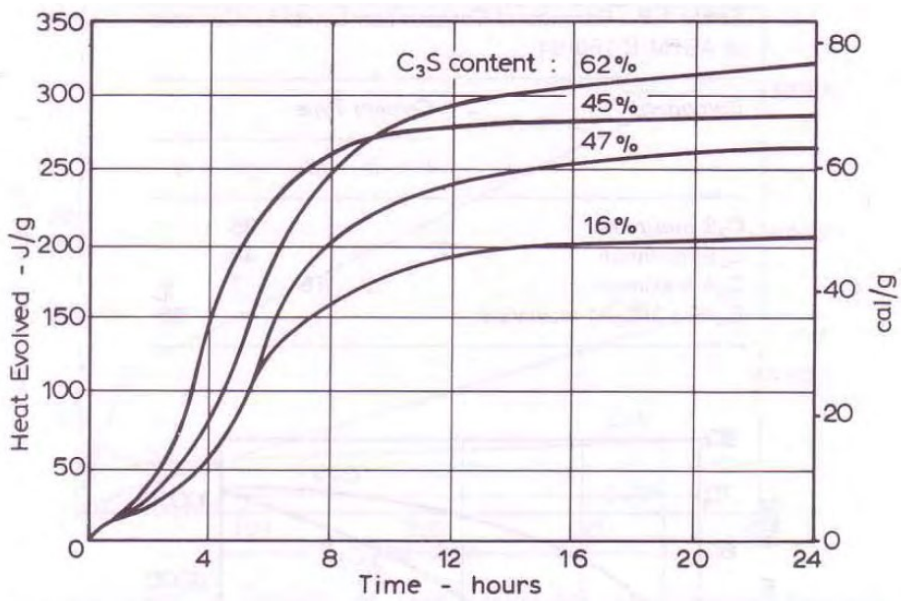

Figure 2-18: Influence of C_3S content on heat evolution (Neville, 1996)

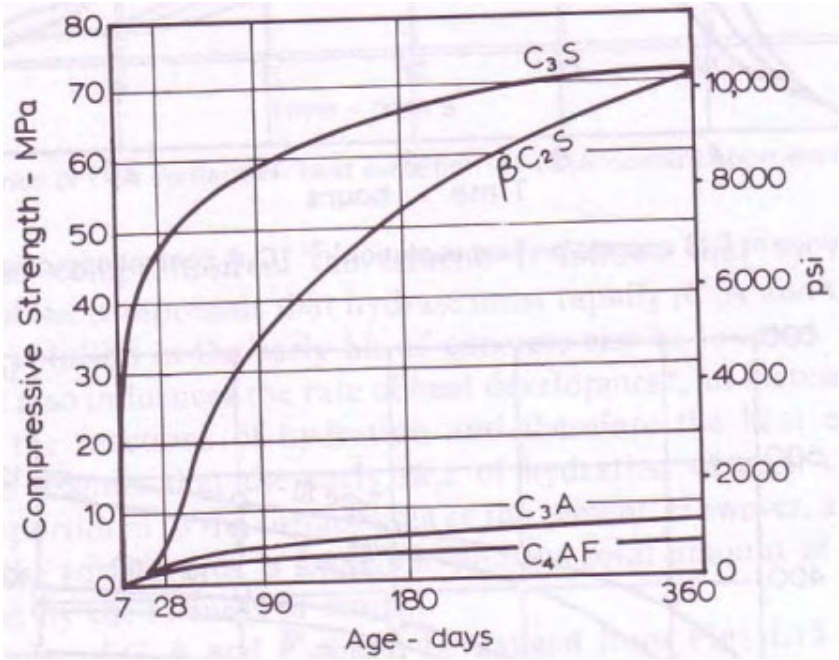

Figure 2-19: Development of strength (Neville, 1996)

2.8 Effective reinforcement ratio

The percentage of effective reinforcement ratio is used in DuCOM-COM3 software. The effective reinforcement ratio according is given by (Construction Ministry of Ethiopia, 2015.) :

$$\rho eff = \frac{As}{Ac,eff} \qquad \text{Eq 2-9}$$

Where Ac,eff = the effective area of concrete in tension surrounding the reinforcement. And Ac,eff = the area enclosed by hc,eff . Based on Figure 2-20, hc,eff is the depth of the tension zone. And hc,eff is the lesser of $2.5(h-d), \frac{(h-x)}{3} and \frac{h}{2}$ as per (Ministry of construction, 2015).

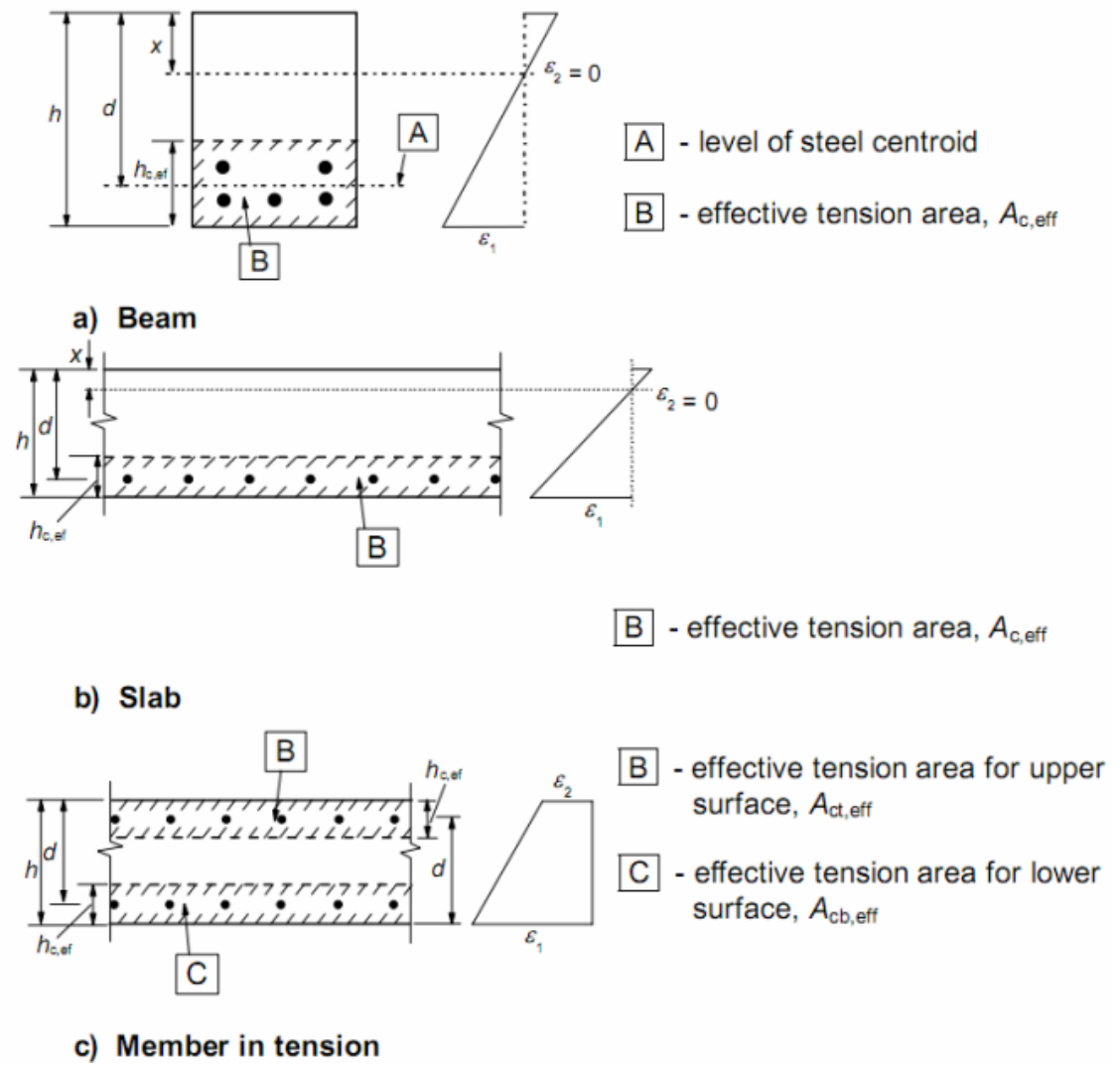

Figure 2-20: Effective reinforcement ratio (Construction Ministry of Ethiopia, 2015)

CHAPTER 3 FINITE ELEMENT MODELLING AND ANALYSIS OF T-GIRDER BRIDGE DECK

3.1 Target structure

The subject of the study is a 20m span T-girder bridge deck at different ambient temperatures and relative humidity under sustaining fixed-point standard truckload.

In order to study the time-dependent deformation behavior of this bridge deck, it has been modeled in a finite element analysis software DuCOM-COM3. For this bridge deck, the design drawings and details of the materials used are presented in Figure 3-1. The design values of geometry and material properties of concrete and reinforcement are used to model the girder in the software. Different modeling parts in the database definition were creating mesh from cube element which is suitable in the software, assigning boundary conditions, defining and assigning materials on different sections to represent actual section behavior, steps, and loading, selecting constitutive built-in time-dependent analysis model, selecting built-in nonlinear criteria in the software, running analysis, history output requests, post-processing analysis.

3.2 Detail of T-girder bridge

Structural design data of the T-girder bridge that was designed in the consulting office (Nomy Engineering Plc,2015) is used for this study. The clear span of this bridge is 2000cm with a 50cm girder seat. The bearing of 30cmx35cmx2.2cm is provided in the design. The center to center spacing of T-girders is 220cm, the thickness of the flange slab is uniform at 22cm, the width of the girder web is also uniform at 45cm and the total depth of girder is 150cm. Due to symmetry, half of the interior T-girder is modeled and analyzed in the software to use the advantage of symmetry and to minimize the time taken to run the analysis of 6624 elements. By taking half of the interior girder, the total number of elements formed is 3312. Boundary conditions in the axis of symmetry are considered to represent the actual behavior of interaction between parts of the T-girder.

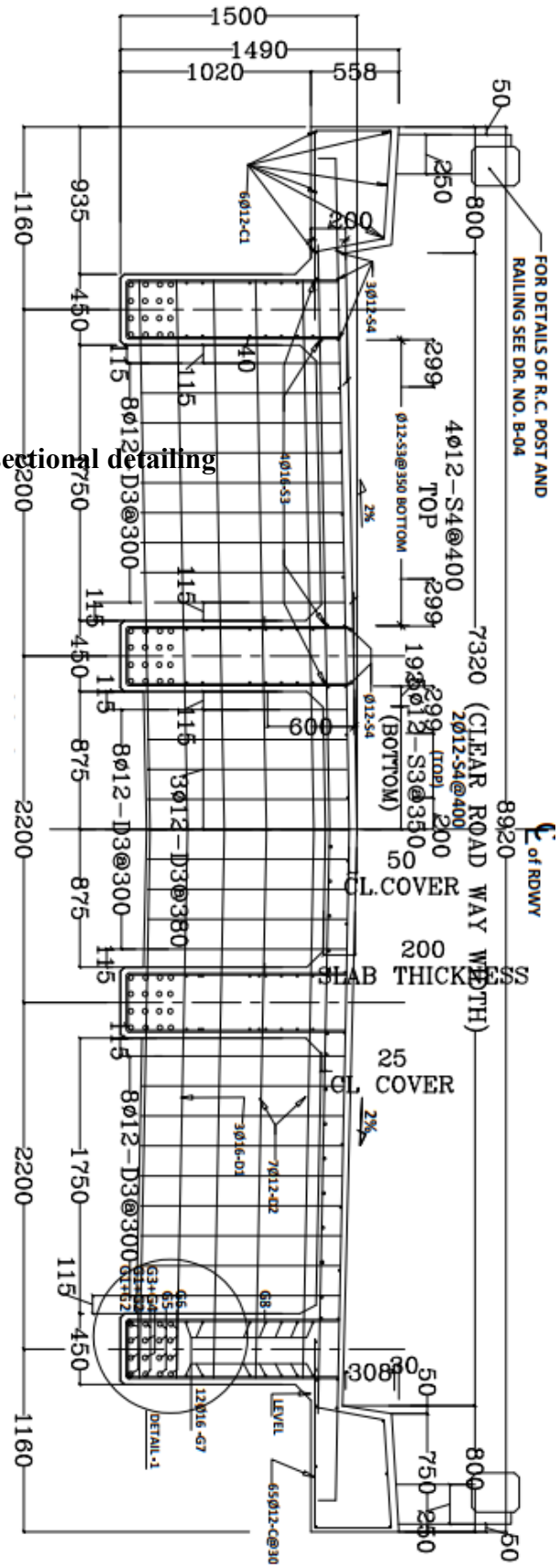

Figure 3-1: T-girder typical cross-sectional detailing

3.3 Use of consistent units in DuCOM-COM3

In DuCOM-COM3 the user need to have to use a consistent unit throughout the modeling of geometry, material definitions, and loading of the model. The output results correspond to the same unit system as the input. The units used in this model kN, cm,day and second.

3.4 Modeling of geometry

The details and dimensions of the girder deck designed by (Nomy Engineering Plc,2015) are used to model the geometry of the deck. A successful working model is the result of correctly modeling both the geometric and material parameters. Taking advantage of the symmetry, only one half of the three- dimensional geometry of interior T-girder is modeled. The cross-sections of the parts are created by using three-dimensional cube geometry provided in the software. After the structure elements are prepared, the corresponding material properties are assigned and section assignment is employed. The mesh size effects on the quality of the results of the analysis are also taken into consideration in selecting mesh size. In order to ensure the analytical accuracy, discretized finite elements with dimensions in the order of mm were set. This T-girder deck model was divided into 50,15,14 elements in longitudinal, transversal and vertical directions, respectively. The geometry of the structure of the frame is as shown in Figure 3-2.

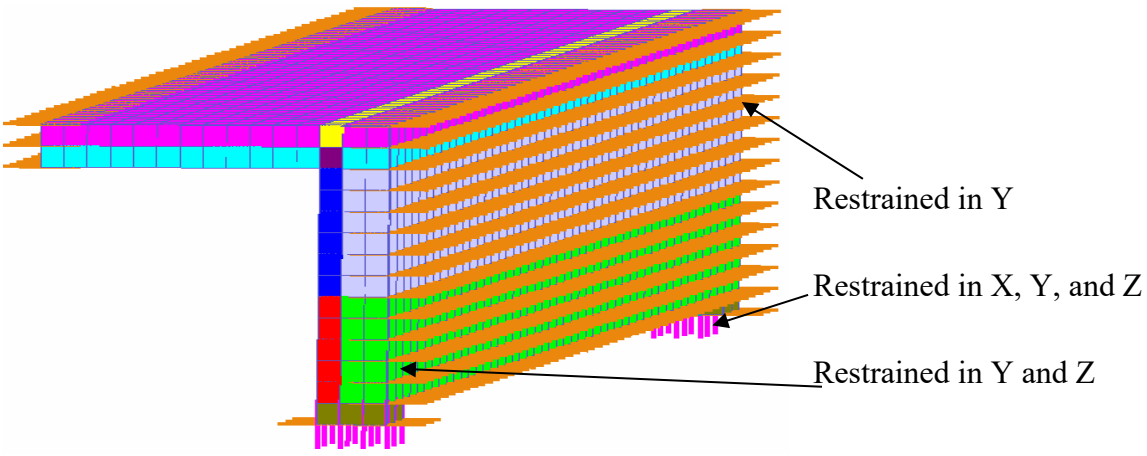

Figure 3-2: Three-dimensional view of the half T-girder model

3.5 Creating the mesh

In DuCOM-COM3, creating the mesh is applied during modeling based on a cube with desired lengths in respective directions. The number of finite elements in the X, Y and Z directions was developed to ensure the analytical accuracy of the structure, discretized finite elements with dimensions in the order of mm were set. Generally, an increasing number of discretized elements will increase the quality of results. After creating the discretized elements of a cube, the half of interior T-girder was created by removing elements that are not desired to form T- girder and a total of 3312 elements were formed as shown in Figure 3-3.

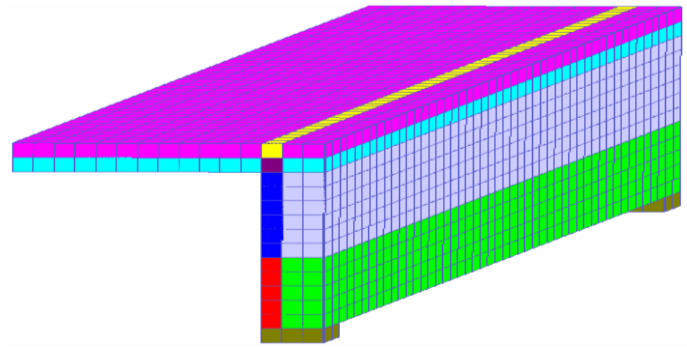

Figure 3-3: Meshed structure

3.6 Defining material properties

Material modeling consists of defining properties of different materials used in the structure. DuCOM-COM3 software has a material definition database where user material properties can be defined. Concrete and steel reinforcement material properties corresponding to the design value are defined. Elastic material property is defined for bearing used in the design to distribute the stress without crushing. This material definition can be handled by using the software interface with the COM3-project material database.

3.6.1 Concrete

The concrete properties used in the analysis of this study are the same as the concrete property used in the design.

Table 3-1: Concrete property used in the model

Initial Modulus of elasticity	24470MPa
Compressive strength	30MPa
Tensile strength	2.6 MPa
Poisson's ratio	0.2
Unit weight	25 $\frac{kN}{m^3}$

To account for the lane load effect, the concrete on the deck surface is increased in a unit weight by including a standard service lane load of 9.34 $\frac{kN}{m^3}$.The increased unit weight of deck surface concrete by accounting service lane load is 34.34 $\frac{kN}{m^3}$.

3.6.2 Mix design used for C30 concrete

The concrete grade employed for the design of this structure is C30 concrete with cubic compressive strength of 30MPa. The mix design for the construction of the structure was as per the procedures and guidelines of (ACI 211, 1991). The same quantity of materials proportion used is incorporated in the software as presented in Table 3-1. The cement is ordinary Portland cement with mineral composition as per Table 3-2.

Table 3-2: Weight of materials

Parameters	Unit weight of coarse aggregates	Unit weight of fine aggregates	Water to cement ratio	Mean size of aggregate with porosity	Entrained air
Value	987.8 kg/m^3	818.9 kg/m^3	54%	0.6	1.50%

Table 3-3: Weight percentage of mineral compounds in Portland cement

Parameters	Alites (C3S)	Belites (C2S)	Calcium aluminate (C3A)	Calcium ferrite (C4AF)	Gypsum
Value	49.70%	23.90%	8.80%	9.40%	3.40%

Table 3-4: Blaine value of powder in cm^2/g

Parameters	Portland cement	Blast furnace slag	Fly ash	Limestone powder
Value	3380	3300	3280	7000

Table 3-5: Specific gravity in g/cm^3

Parameters	Gravel	Sand	Cement	Slag	Fly ash	Limestone powder
Value	2.62	2.58	3.15	2.9	1.93	2.15

To validate the mix design, a cube element with dimensions of 15cm was modeled in DuCOM-COM3. To model the actual behavior of the hygro-thermal reaction at the face of the specimen with environmental conditions, the software has a special feature, Trans elements.

a) b)

Figure 3-4: Cube element a) without Trans elements b) with Trans elements

3.6.3 Reinforcement

Elastic material property is assigned to steel as the stresses in the steel during the analysis are expected to remain well under the elastic limit. The reinforcement bars are embedded in the concrete by the assumption of the full bond between concrete and reinforcement bars. The properties of the reinforcement material assigned in the model based on the design.

Table 3-6: Reinforcement property used in the model

Initial Modulus of elasticity	200000MPa
Yield strength	420 MPa
Tensile strength	600MPa
Poisson's ratio	0.3
Unit weight	$77\ \frac{kN}{m^3}$
Tension rupture strain	0.12

Tension rupture strain up to 14% is recommended (P.Park&T.Paulay,1975).

3.7 Effective reinforcement ratio.

COM3 software takes the reinforcement effective to surrounding concrete. An effective reinforcement ratio is the ratio of the area of reinforcement to surrounding concrete. Based on the formula by (Construction Ministry,2015), the effective reinforcement ratio can be calculated as:

$$\rho_{eff} = \frac{As}{Ac_{,eff}}$$

$Ac_{,eff}$ is the area enclosed by h_{eff}

$$h_{eff} \le \left\{ 2.5(h-d), \frac{(h-x)}{3} and \frac{h}{2} \right.$$

Based on the design data from Figure 3-1, $h-d = 213\,\text{mm}$

$2.5(h-d) = 2.5x213 = 532.5\,\text{mm}$

Width of the girder, $b_w = 450\,\text{mm}$

$Ac_{,eff} = 450x532.5 = 239,625\,\text{mm}^2$

As= 24ϕ32mm =19296mm^2, main reinforcement in girder section in the X-direction,

$\rho_x = \frac{19296}{239625} X100 = 8.051\%$ with tension stiffening factor of 0.4

On the slab part, there is 136 ϕ16mm reinforcement.

$As = 2\phi 16c / c130 = 3092.3mm^2$ in 1000mm

$Aeff = heff * b$

$heff = 2.5(c + \frac{\phi}{2}) = 2.5(25 + \frac{16}{2}) = 82.5mm$

c = is the center of concrete cover

$\rho_y = \frac{3092.3}{82.5*1000} X100 = 3.748\%$ with tension stiffening factor of 0.4

For stirrups provided within diaphragm with the spacing of 1805mm.

$As = 3379.68mm^2 in 1805mm$.

$Aeff = heff * b$

$heff = 2.5(c + \frac{\phi}{2}) = 2.5(25 + \frac{12}{2}) = 77.5mm$

$\rho_y = \frac{3379.68}{77.5 * 1805} X100 = 2.416\%$ with tension stiffening factor of 0.4

3.8 Assigning material properties to girder sections

After the mesh is created and finite elements that are not representing the T-girder are removed, the materials are defined and assigned in the section to represent actual section property. Depending on the position and amount of reinforcement present in the girder different material properties are defined and assigned. In DuCOM-COM3 software, the reinforcement ratio is incorporated as an effective reinforcement ratio based on the effective stress at the surrounding concrete.

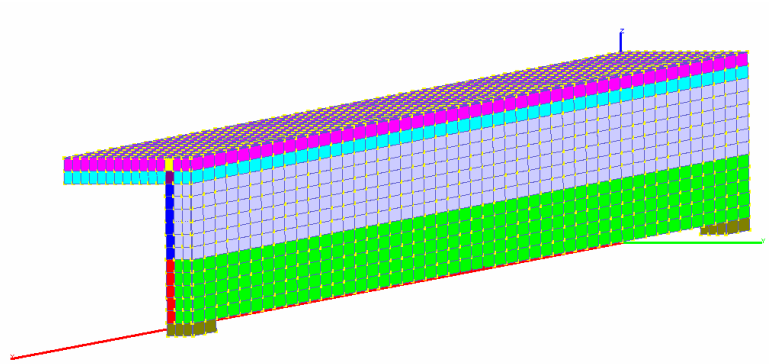

Figure 3-5: Sections with different material properties

Yellow = Concrete with $\phi 12$ stirrups and $\phi 16$ longitudinal reinforcements, $\rho_X = 1.37\%, \rho_y = 3.748\%$ and $\rho_z = 2.34\%$ with tension stiffening factor of 0.4

Red = Girder section with $\phi 12$ stirrups and $\phi 32$ main longitudinal and $\phi 16$ skin reinforcement, $\rho_X = 8.051\%$ and $\rho_z = 2.416\%$ with tension stiffening factor of 0.4 and tension softening factor of 2 in the Y-direction

Gray = Unreinforced section with tension softening factor of 2 in all directions.

Blue = Girder section with $\phi 12$ stirrups and $\phi 16$ skin reinforcement, $\rho_X = 1.378\%$ and $\rho_z = 2.416\%$ with tension stiffening factor of 0.4 and tension softening factor of 2 in the Y-direction.

Purple = Concrete section by including surface lane load effect as unit weight, $\rho_X = 1.37\%$ and $\rho_y = 3.748\%$ with tension stiffening factor of 0.4 and tension softening factor of 2 in the Z-direction.

Green = Girder section with only main longitudinal reinforcement, $\rho_X = 8.051\%$ with tension stiffening factor of 0.4 and tension softening factor of 2 in both Y and Z-directions.

Dark purple = Girder section with $\phi 16$ deck reinforcement and $\phi 12$ stirrups, $\rho_y = 3.748\%$ and $\rho_z = 2.416\%$ with tension stiffening factor of 0.4 and tension softening factor of 2 in the X-direction.

Cyan = Girder section with $\phi 16$ deck reinforcement, $\rho_y = 3.748\%$ with tension stiffening factor of 0.4 and tension stiffening factor of 2 in both X and Z-directions.

Dark green = Elastic plate to represent girder seat bearing

If reinforcement bars are in the section, tension stiffening factor of 0.4 is used in the direction of reinforcement while tension softening factor of 2 is used in the direction where the section has no reinforcement. These values are in the research work for coefficients for tension stiffening/softening (Maekawa et al., 2003). Depending on the presence of reinforcing steel in the section, different material properties are assigned as shown in Figure 3-5.

3.9 Restraint conditions

Once the mesh is created and the desired structural system is formed in DuCOM-COM3, restraint conditions need to be assigned to model the actual behavior of one-half section of the T-girder. The longitudinal length is modeled in X-direction whereas the transversal length is modeled in Y-direction but the depth of the girder is modeled in the Z direction. The girder seat is modeled by the elastic material property to represent the girder seat

bearing plate. The boundary conditions are simple supports for the nodes at the end of the girder. Displacements in longitudinal, transverse and vertical directions are restrained at one side and only transverse and vertical displacements are restrained at the other side (Figure3-2).

3.10 Defining steps and loading

The loadings considered in the analysis are sustained load due to the dead load of the girder and the deck slab and moving wheel load. The effect of temperature and relative humidity on the creep and shrinkage in the girder elements is considered by incorporating input materials and environmental conditions. The step and load interface in DuCOM-COM3 are used to define the analysis steps and loading. Since the current study involves evaluating the time-dependent deformation behavior of the bridge deck, it is important to define several steps in order to capture the behavior of the structure at different periods of time. For this study, 213 steps are defined where the first 42 steps are subdivisions of 1day at which material is isolated, no effect of environmental conditions (ambient temperature and relative humidity), the other 51 steps are subdivisions of 7 days in which there were sufficient watering and the effect of ambient temperature and relative humidity, the 150^{th} step is the load effect at 28days after construction and the next 103 steps are subdivisions of 1 year. The remaining 16 steps are at the interval of 1 year. Thus, the number of evaluations corresponds to immediately after the loading which is at 150 days, 1 to 11 months, 1 year, 2-3 years, 4-6 years and 7-16 years. A total of 16 years of deformation behavior is evaluated in this research.

The loading on the girder is not imposed at the same time. The loading was done step by step in four steps. In the first step, only the dead load of the structure is applied. To activate the dead load effect, DuCOM-COM3 software has a special treatment by defining acceleration of gravity in Z-direction in a unit of a centimeter (cm) and second (s). In this model, the activation is based on the DuCOM-COM3 inbuilt value of the acceleration of gravity of $980cm/s^2$ in Z-direction. Based on this value, the software takes the effect of own weight in the direction of acceleration of gravity. If this value is being zero, the software will neglect the effect of dead load and take only imposed live load.

In this study, the standard imposed truck wheel load of 145kN and 35kN based on (AASHTO,2002) were applied in four steps by dividing into equal parts. To prevent the local failure due to concentrated loading, the load in each step is loaded in two adjacent neighboring nodes. For fixed-point load, the positions of the loads were at the standard distance of the truck wheel load where the central load at the center of the bridge while the others were outside of the center (Figure 3-6). In the case of moving truck wheel load, the load was applied by simultaneous loading and unloading two adjacent and two previous nodes at every four loading steps.

$P = \frac{145kN}{2} = 72.5kN$, $\frac{P}{4} = \frac{145kN}{8} = 36.25kN$ service load.

Standard lane load of $9.34\ \frac{kN}{m^2}$.

Different steps after analysis help to follow the change in deflection due to sustained loading with time.

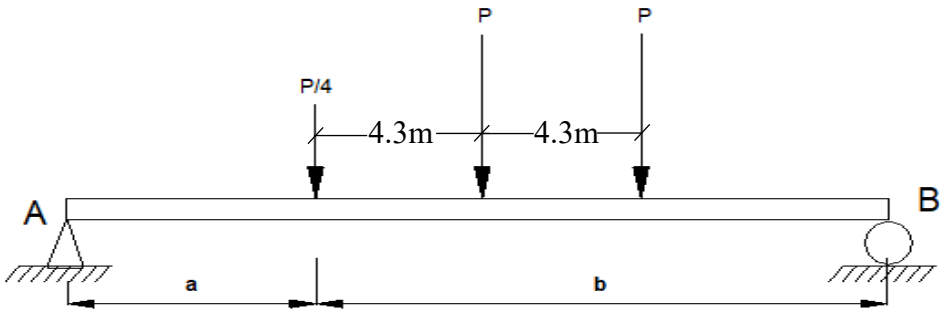

Figure 3-6: Structural configuration for fixed-point loading positions and layout

Table 3-7: Loading position for maximum deflection

Load	a	b	$\frac{L}{2} = X$
P/4	4.303	15.697	10.25
P	8.603	11.397	10.25
P	12.903	7.097	10.25

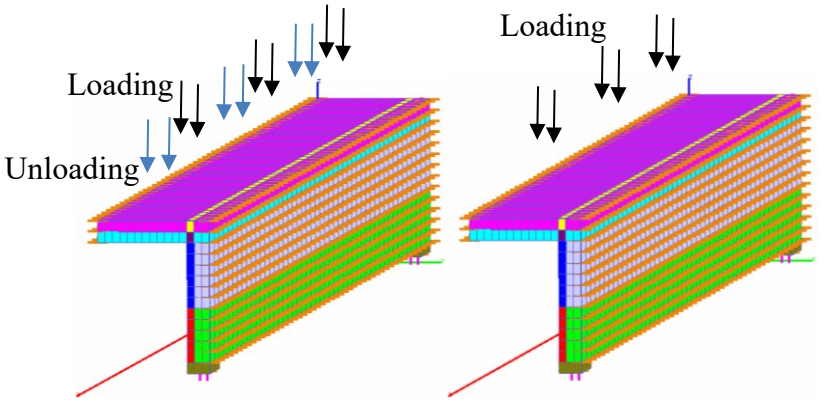

a) Moving load model b) Fixed point load model

Figure 3-7: Loading model in COM3

3.10.1 Influence lines for shear force and bending moment

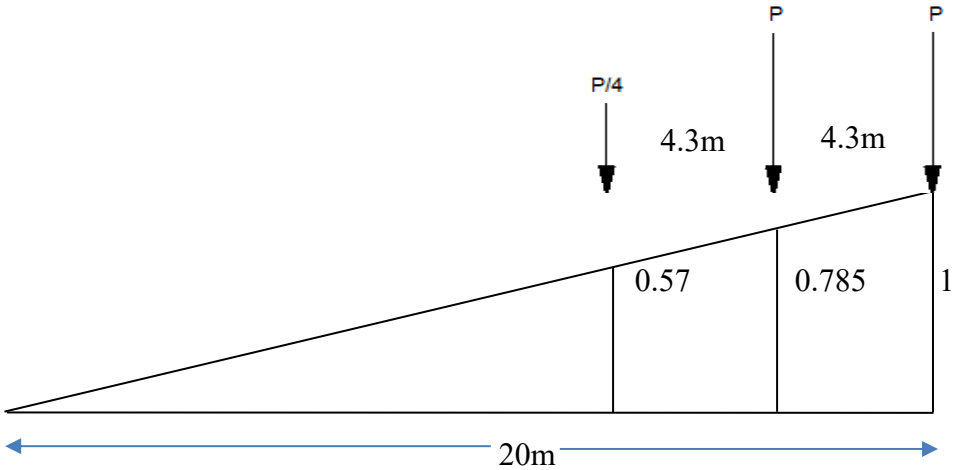

Figure 3-8: Influence line diagragm for shear force

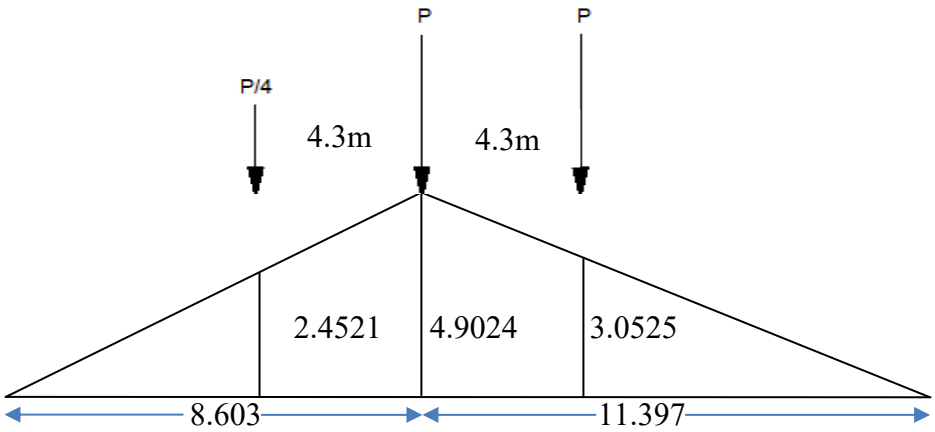

Figure 3-9: Influence line diagragm for bending

3.10.2 Modeling trans elements

Trans elements are features in DuCOM to model the media for hydro-thermal transfer on the surface of the structure. These elements are used to model the actual response of the structure to environmental conditions.

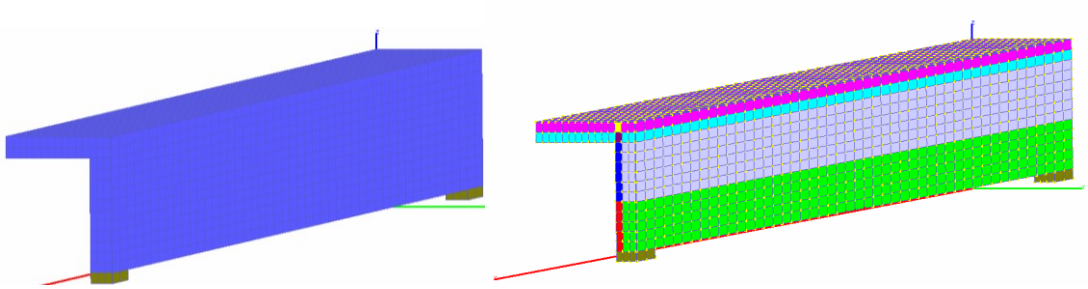

a) b)

Figure 3-10: Section model a) with trans elements b) without trans elements

3.10.3 Including time-dependent analysis

Long term deformation effect is based on inbuilt concrete time-dependent analysis constitutive models in DuCOM-COM3. The characteristics of the time-dependent constitutive model in this software are that the hygro-states of the moisture trapped in pores of material in the scale of [nm] to [μm] scales and then coupled with the effect of structural behavior.

3.11 Ambient temperature and relative humidity

The local temperature and relative humidity were obtained from 30 years Ethiopian Meteorological Institute data for Addis Ababa and Semera as shown in **Table 3-7** and **Table 3-8** respectively. The annual average temperature was 23.51°C and relative humidity of 64.2% for Addis Ababa. The annual average temperature was 34.34°C and relative humidity of 47.73% for Semera.

Table 3-8: Ambient temperature and relative humidity patterns for Addis Ababa

Month	Jan	Feb	Mar	Apr	May	Jun	Jul	Aug	Sep	Oct	Nov	Dec
T (°C)	23.9	25.1	25.4	24.8	25.2	24	21	21	22.1	23	23	23
RH (%)	58.9	45.2	47.7	57.9	65	68	74	83	76.5	71	66	58

Table 3-9: Ambient temperature and relative humidity patterns for Semera

Month	Jan	Feb	Mar	Apr	May	Jun	Jul	Aug	Sep	Oct	Nov	Dec
T (°C)	35.9	36.3	36.1	34.3	39.2	33	31	30	34.1	33	34	36
RH (%)	35.8	30.1	32.3	47.2	41.8	47	58	61	59.9	59	53	48

3.12 Running analysis

The analysis was done by running a coupled analysis integrating moisture kinematics that numerically models hydration reactions, pore structure formation, moisture migration with a material-structure response analysis based on a nonlinear material constitutive law. The thermo-hydro dynamic analysis at the microscopic level is integrating the phenomena of moisture movement and solid-liquid equilibrium within micropores of different scales to compute temperature,degree of hydration,porosity, saturation, viscosity and pore pressure at all gauss points of the mesh. Volumetric stress in a cement paste and mositure migration are predominant mechanisms for creep in concrete.

3.12.1 Creep Mechanics

Creep of concrete originates in the hardened cement gel that contains capillary pores through the following mechanisms (Maekawa et al., 2003).

Volumetric stress in a cement paste induces an instantaneous elastic deformation given by:

$$\sigma_{cp} = E_e \varepsilon_e \qquad \text{Eq 3-1}$$

$$E_e = \frac{dK_{cp}}{d\psi}$$

Where:

σ_{cp} = volumetric stress in a cement paste

E_e = volumetric stiffness of the elastic spring

ε_e = instantaneous elastic strain

K_{cp} = the volumetric stiffness of the cement paste

ψ = degree of saturation of micro pores

The short-term creep behavior caused by moisture migration with in capillary pores at a time t is given by:

$$\sigma_{cp} = E_c \varepsilon_c + E_c C_c \frac{d\varepsilon_c}{dt} \qquad \text{Eq 3-2}$$

$E_c = a_{ec} E_e f(S_{cap})$,the recommended value of a_{ec} is 3.

$f(S_{cap}) = \exp(0.69(S_{cap} - 1)$

Where:

E_c = volumetric stiffness of the visco-elastic spring

ε_c = visco-elastic strain

C_c = viscous coefficient related to condensed water motion with in capillary pores.

$$C_c = \frac{a.f(S_{cap}).\eta}{\phi_{cap}} \qquad \text{Eq 3-3}$$

a = dashpot constant for visco-elastic part that varies with degree of saturation. Its recommended value is 4.3×10^{-3}.

ϕ_{cap} = capillary porosity

S_{cap} = saturation of capillary pores

η = viscosity of micropore water

Moisture kinematics with in gel pores at a constant applied stress induce visco-plastic strain which is the main part of time-dependent unrecoverable long-term creep. Plastic strain increases with time and may attain convergence point.This creep mechanism is given by:

$$\frac{d\varepsilon_g}{dt} = \frac{(\varepsilon_{g\lim} - \varepsilon_g)}{C_g} \quad \text{Eq 3-4}$$

$$C_g = d.f(S_{gel}).\eta.\phi_{gel} \quad \text{Eq 3-5}$$

$$\varepsilon_{g\lim} = f_1(\sigma_{cp}).f_2(S_{gel}) \quad \text{Eq 3-6}$$

$$f_1 = \frac{\sigma_{cp}}{E_g}$$

$$E_g = \frac{E_e}{4}$$

$$f_2 = \exp(-a.S_{gel})$$

Where:

$\varepsilon_{g\lim}$ = plastic strain limit at convergence

S_{gel} = degree of saturation of gel pores

ϕ_{gel} = gel porosity of cement paste

d = dash pot constant for visco-plastic part that varies with degree of hydration. Its recommended value is 0.9.

Moisture kinematics with in interlayer pores causes instantaneous volume change. This plastic strain is related with the motion and dissipation of interlayer water at time t.

$$\frac{d\varepsilon_l}{dt} = \varepsilon_p \phi_{\text{int}} \frac{dS_{\text{int}}}{dt} \qquad \text{Eq 3-7}$$

Where:

ε_l = moisture related instantaneous plastic-strain

S_{int} = saturation of interlayer pores

ϕ_{int} = porosity of interlayer

ε_p = plastic strain per unit of porosity

The total strain of solidifying cement paste at time t thus can be computed by:

$$\varepsilon'_{cp}(t') = \varepsilon_{cp}(t) - \varepsilon_{cp}(t') \qquad \text{Eq 3-8}$$

$$\varepsilon'_{cp} = \varepsilon_e + \varepsilon_c + \varepsilon_g + \varepsilon_l \qquad \text{Eq 3-9}$$

Where:

t' = time at which a cement paste is solidified.

ε'_{cp} = total strain in cement paste

Volumetric stress of cement paste is resisted by skeleton and pore water pressure of cement paste composite .

$$\sigma_{cp} = \sigma'_{cp} + \beta\sigma_s \qquad \text{Eq 3-10}$$

σ'_{cp} = stress on a cement skeleton

σ_s = pressure drop in pore water

β = Moist volume fraction. For fully occupied space β is unity.

$$\sigma'_{cp}(t) = \int_{t'=0}^{t} \sigma_{cp}(t',t)\, d\psi(t') \qquad \text{Eq 3-11}$$

$$\psi(t) = \frac{V(t)}{V_{cp}}$$

Where :

$\psi(t)$ = degree of hydration at time t

$V(t)$ = hydrated volume of cement at time t

V_{cp} = total volume of cement available for hydration

$$\sigma_s = \frac{-2\gamma}{r_s} \qquad \text{Eq 3-12}$$

$$\sigma_s = \frac{-\rho RT}{M} \ln h$$

Where:

γ = water surface tension

r_s = pore radius

R = universal gas constant

T = temperature

M = molecular mass of water

h = relative humidity of the vapour in equilibrium with condensed water

$$\beta = \frac{\phi_{cap} . S_{cap} + \phi_{gel} . S_{gel}}{\phi_{cap} + \phi_{gel}} \qquad \text{Eq 3-13}$$

Where:

ϕ_{cap} = capillary porosity

ϕ_{gel} = gel porosity

S_{cap} = capillary pores saturation

S_{gel} = gel pores saturation

This coupling is a key parameter implimented in DuCOM-COM3 to integrate thermo-hydro dynamics and deformational mechanics of concerete structures.

After all the steps and loads in COM3 were defined with temperature and relative humidity in DuCOM at the same time step as COM3, link analysis was activated in DuCOM-COM3. To complete the link analysis of the model, it took more than 8 hours.

3.13 Running Post Processing analysis

The results can be displayed after running the post-processing analysis. DuCOM-COM3 has a processor for post-processing the results from the analysis. Post-processing of the model was done using the interface of process COM3 result data for structure result display and for material property post-processor, DuCOM result data is available.

3.14 Displaying the results

In COM3, accessible results are nodal results of reaction-displacement and nodal displacement-time relationships and element-wise results of deformed shape contour, contour for the crack pattern, reaction-displacement, stress-time, strain-time, stress-strain relationships, principal stresses, and principal strains

In DuCOM, accessible results are the heat of hydration, relative humidity, degree of hydration, degree of saturation, water content, compressive strength, shrinkage, and porosity.

Contours – The variables, such as stress, strain, crack, and displacement, can be represented as a contour in the model for any increment in a step by different contours colors.

Deformed shape – The nodal deformation pattern of the model can be examined in detail using the display COM3 result command. From the deformed shape, the long-term deflection and cracking of the concrete structure can be evaluated for any increment in a step.

Displacement-time data – The displacement -time data can be read and plotted from the COM3 result in the output database obtained from analysis results. Time can be average time, logarithmic time or step. The outputs requested after the analysis are available and can be recorded for an element, nodes, and integration points. Tabular data from the displacement-time data can be created, saved and/or copied to excel or any other program for further analysis.

Stress and strain-time data – The stress and strain -time data can be read and plotted from the COM3 result in the output database obtained from analysis results.

CHAPTER 4 RESULTS AND DISCUSSION

The multi-scale simulation of time-dependent deformation behavior of the T-girder bridge has been carried out using DuCOM-COM3 software. The results obtained from the analysis are presented and compared with the previous findings in this section. Heat generation, degree of hydration, degree of saturation, pore water content, shrinkage strain, compressive strength for both specimen and girder deck are plotted. And strain and mid-span deflection in the girder are plotted. The simulation was for a 16-years age girder starting from casting.

The effects of sustained load and environmental conditions at different ages of the girder after hardening on the system are compared and presented here. It is observed that the deformation of girder after loading significantly increases in the first 2-3 years and the increment is gradual after 3 years. This finding is in a very well agreement with the finding by (Neville, 1996) where they stated that the time-dependent deformation due to creep and shrinkage is significantly increasing at an increasing rate within 2-3 years accounting with about 90% of the total deformation.

In this study, as shown in Figure 4-13 the rate of increment in deformation is significant within 3 months attaining about 92% of a 1-year deformation. From the figure, one can note that there is still a significant increase in deformation. This behavior confirms the finding by (Gilbert et al., 2010) where they come up to the conclusion that the limit of time-dependent deformation is at the time of infinity.

4.1 Results of Cube Specimens at different ambient temperature and relative humidity

To validate mix design consistency, a cube specimen of dimensions of 15cm was modeled and analyzed under the effect of relative humidity and ambient temperature for Semera and Addis Ababa.

4.1.1 Results of mix heat generation

The same cube specimen at different temperatures and relative humidity showed a significant difference in heat generation. As expected, the exothermic heat of reaction is increased when ambient temperature increases and relative humidity decreases as shown

in Figure 4-1. Witness in Figure 4-1, the internal heat of reaction is more than 38°C for Semera (temperature 34.3°C and relative humidity 47.7%). Whilst, the heat generation is about 26 °C for Addis Ababa (ambient temperature 23.5°C and relative humidity 64.2%).

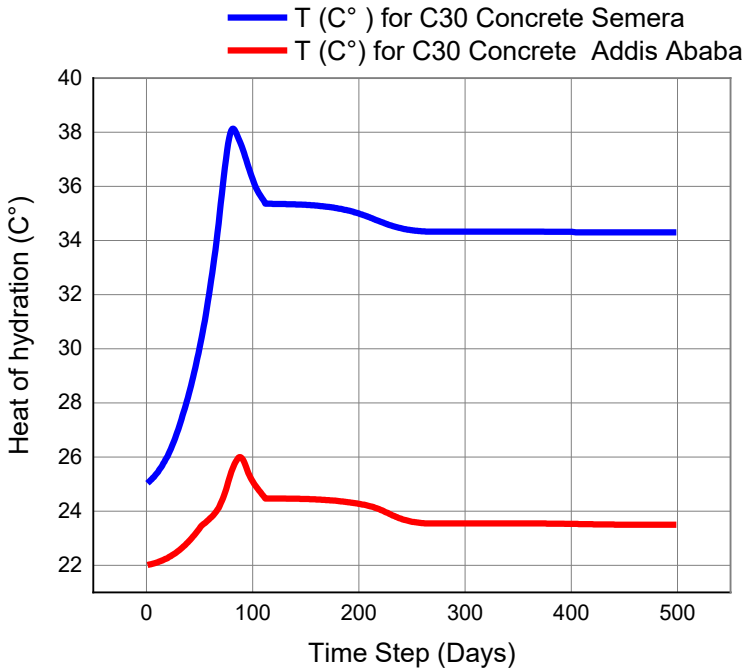

Figure 4-1: Comparison of variation of heat generation under different ambient temperature and humidity conditions

4.1.2 Results of pores water content

The water content in the interlayer pores decreases when water expel from the paste as temperature increases. For mix design in Semera (at temperature of 34.3°C and RH of 47.7%), the amount of water remaining in the concrete is less than 40Kg/m^3 after 1 year of hardening whereas this value is about 125Kg/m^3 for mix in Addis Ababa (at temperature and RH of 23.5°C and 64.2% respectively) as shown in Figure 4-2. With this environmental effect, more than 68% of water was lost from the concrete for Semera and results in a lower degree of hydration as shown in Figure 4-2 and a significant reduction in strength property as compared to the properties of the same concrete in Addis Ababa.

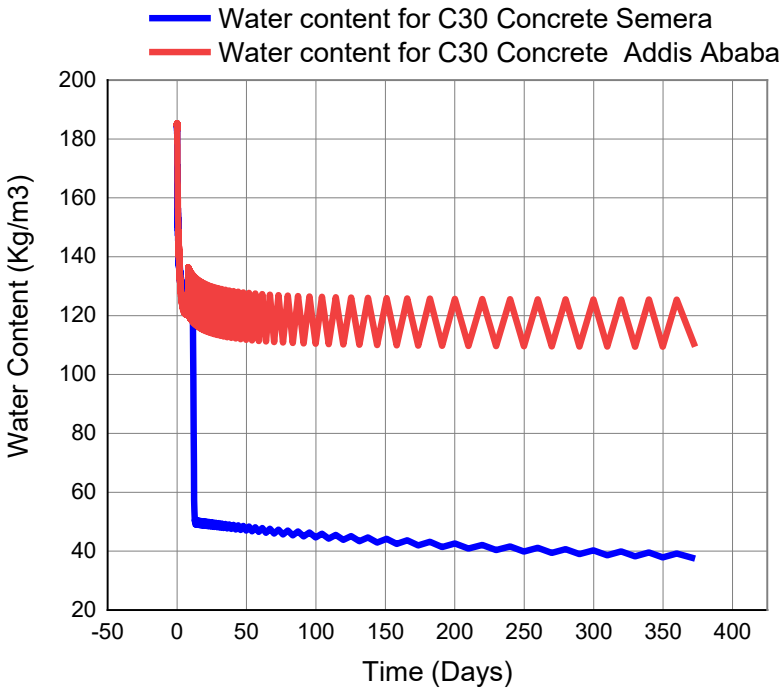

Figure 4-2: Comparison of pore water content at different ambient temperature and RH

4.1.3 Results of saturation of interlayer pores

Witness in Figure 4-3, as relative humidity increases the interlayer pores saturation increases and hydration progresses with time. On the other hand, when the relative humidity decreases, the interlayer saturation also decreases results in the instantaneous plastic strain, capillary viscoelastic strain, gel plastic strain and interlayer plastic strain caused by the loss of interlayer water increases as temperature increases. This phenomenon is in good agreement with finding by (Asamoto et al., 2006). The dispersion of moisture due to temperature increase and decrease in relative humidity promotes the varying moisture in capillary and gel pores because of the viscosity and creep formation depends on pore saturation. As shown in Figure 4-3, the computed relative humidity inside pores is decreasing and reaches about 47.7% in equilibrium with environmental relative humidity. This drop of internal relative humidity is due to self-desiccation. The general form of the result of Figure 4-3 for Semera with temperature 34.3°C and relative humidity of 47.7% is consistent with finding in (Ishida et al., 2018).

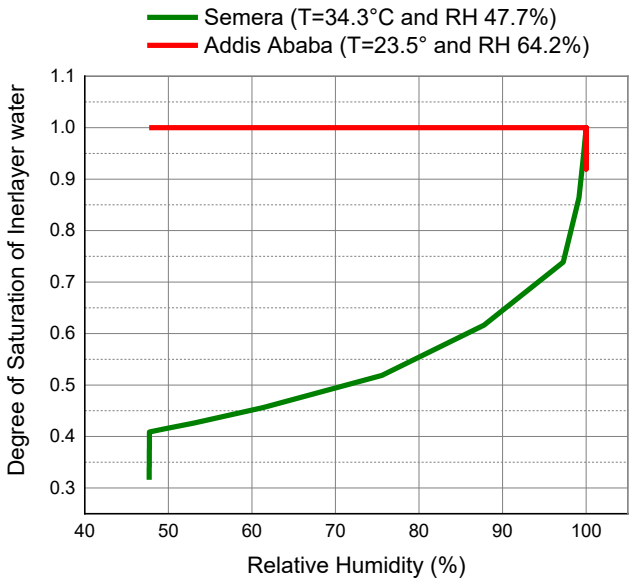

Figure 4-3: Comparison of interlayer pore water at different ambient temperature and relative humidity

Witnessed in Figure 4-4, the degree of saturation of interlayer pores is significantly decreasing for concrete at Semera (T=34.3°C and RH=47.7%) from 100% at the beginning to about 33% whilst the reduction for Addis Ababa (T=23.5°C and RH=64.2%), is negligible, which was at the beginning (92%) and then came to equilibrium.

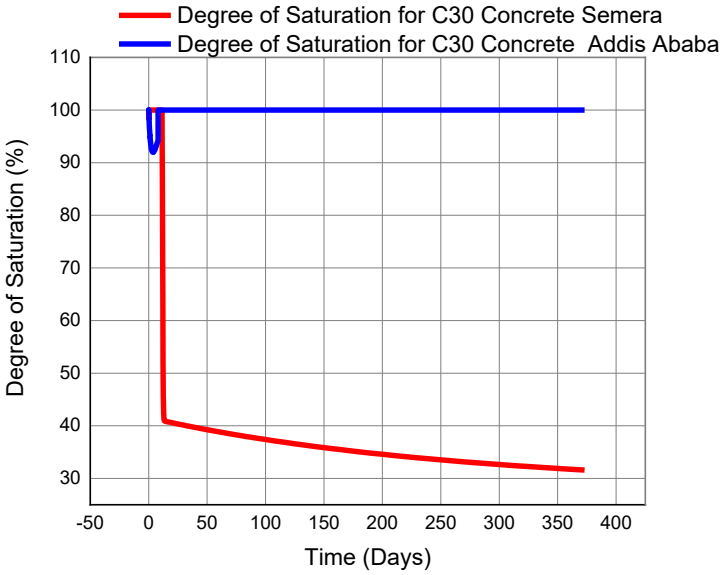

Figure 4-4: Comparison of the degree of hydration at different ambient temperatures and relative humidity.

4.1.4 Results of the degree of hydration

Due to moisture loss from concrete as temperature increases, there is a significant difference in hydration. Incomplete hydration is one of the mechanisms for long term deformation of concrete decks. From Figure 4-5, it can be noted that when temperature increases and relative humidity decreases, some cement particles remain un hydrated due to high heat generation at early age shown in Figure 4-1 that causes the moisture loss from cement paste.

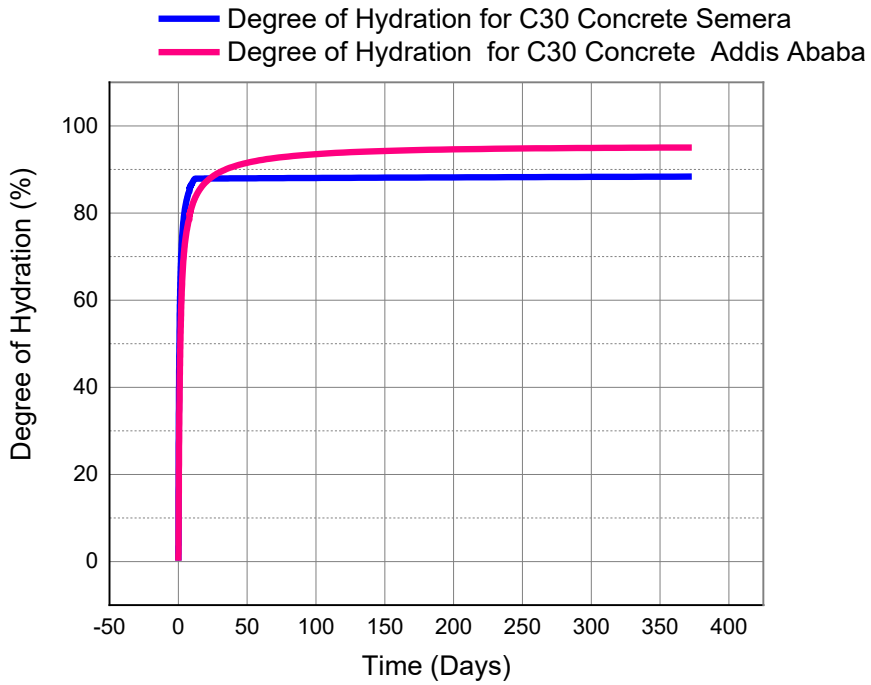

Figure 4-5: Comparison of the degree of hydration under the effect of ambient temperature and relative humidity

4.1.5 Results in Porosity and pore size distribution

Pore formation in concrete significantly influences the strength properties of the concrete. Based on the pore ratio result of Figure 4-6, it can be noted that the capillary, effective and total pore ratio are generally varying with time at different temperature and relative humidity. The variation of capillary pores is more significant as compared to variation in total and effective pores. When porosity increases, stress concentration will be on the solid skeleton and this significantly influences the long-term creep.

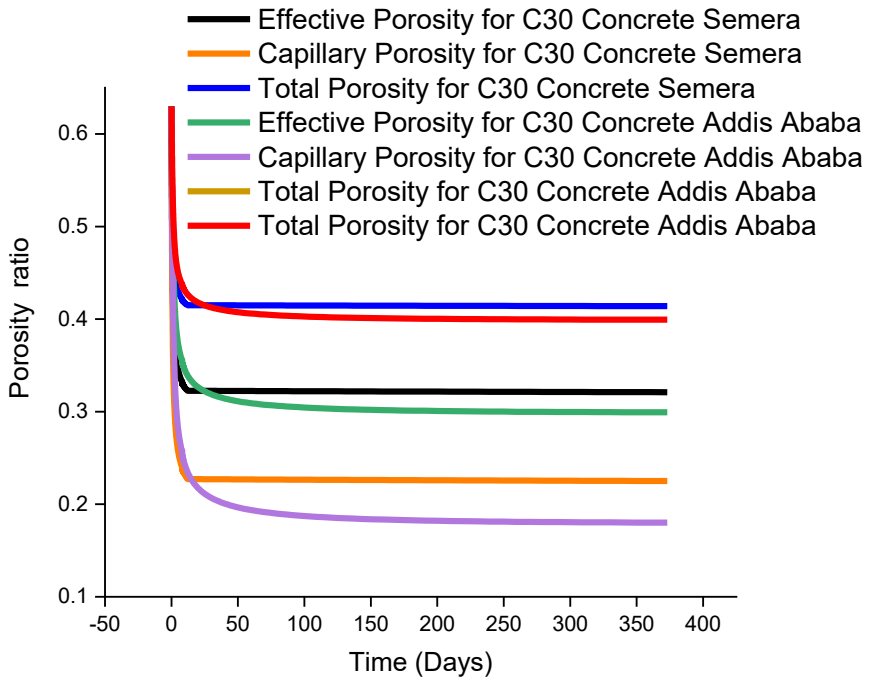

Figure 4-6: Pores size distribution at different temperature and RH

4.1.6 Results of shrinkage strain

Regarding drying shrinkage, higher temperature leads to greater shrinkage. As shown in Figure 4-8, the shrinkage strain was significantly increased when temperature increases and relative humidity decreases. The graph in Figure 4-7, showed that the instantaneous plasticity of interlayer pores is directly associated with the saturation. In the beginning, the interlayer pores are closed to water molecules in size. Later on, the moisture loss from the pores causes the interlayer space to be closed due to the strong surface energy of calcium-silicate hydrates and resulting in instantaneous contraction. Similar material behavior is observed in research by (Maekawa et al., 2003). For Semera (temperature of 34.3°C and RH of 47.7%), as shown in Figure 4-7 again, when the interlayer saturation is 100%, the shrinkage is nearly zero while the shrinkage strain of 8300×10^{-6}cm/cm occurred when the interlayer saturation reduced to 35%. However, as shown in Figure 4-8, the shrinkage for Addis Ababa is found negligible as more than 95% of the degree of hydration was attained (Figure 4-5). As can be seen from Figure 4-8, the rate of shrinkage is considerably increased in the initial phase of drying.

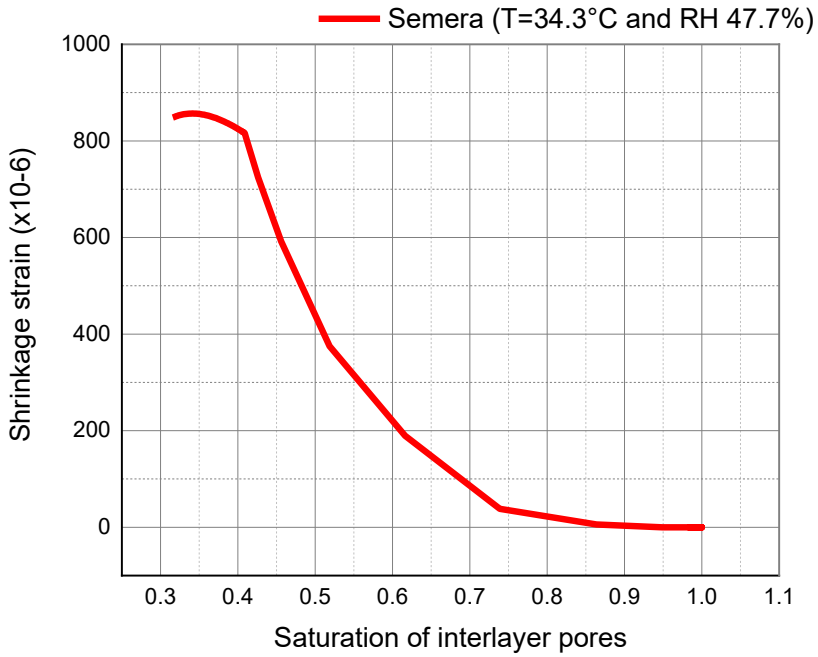

Figure 4-7: Relationship between the saturation of interlayer and shrinkage by loss of interlayer water

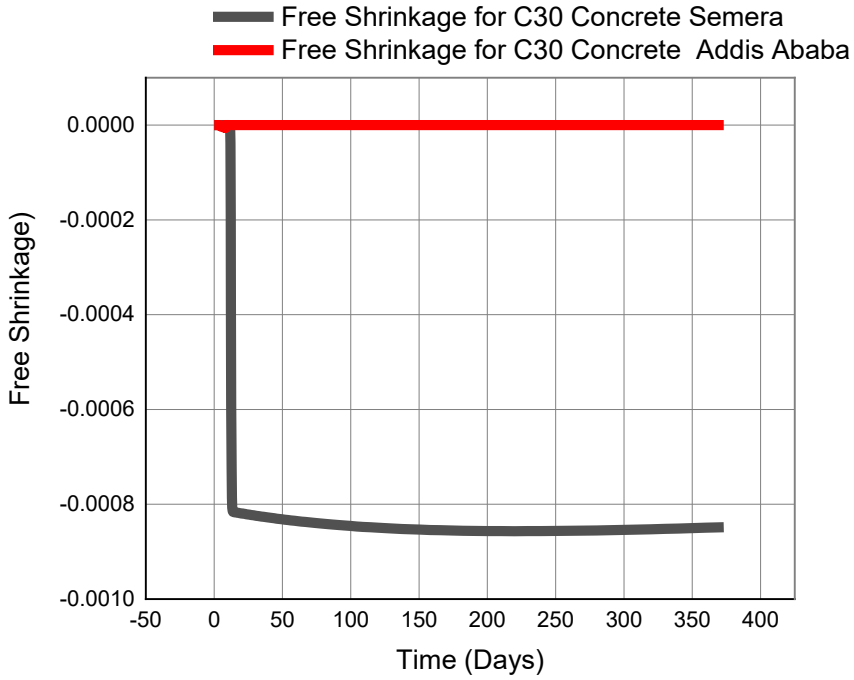

Figure 4-8: Comparison of shrinkage strain at different ambient temperature and relative humidity

4.1.7 Results of compressive strength

The compressive strength is the result of the combined effect of microstructure formation and moisture migration. As shown in Figure 4-9, the compressive strength of concrete increases when the ambient temperature is low and relative humidity is high and vice versa. After a long time, the strength increase is not significant. This finding is in line with the findings reported in (Ishida et al., 2018) and (Maekawa et al., 2003).

With the same mix proportion, the maximum compressive strength attained at an ambient temperature of 23.5°C and relative humidity of 64.2% is about 42MPa whilst the maximum compressive strength attained at a temperature of 34.3°C and relative humidity of 47.7% is about 30MPa. This significant reduction is due to shrinkage strain at an early age and incomplete hydration resulted in porous concrete. As creep is inversely proportional to the strength of concrete, the creep deformation of the bridge deck at Semera is thus considerably increased when compared to deformation behavior at Addis Ababa.

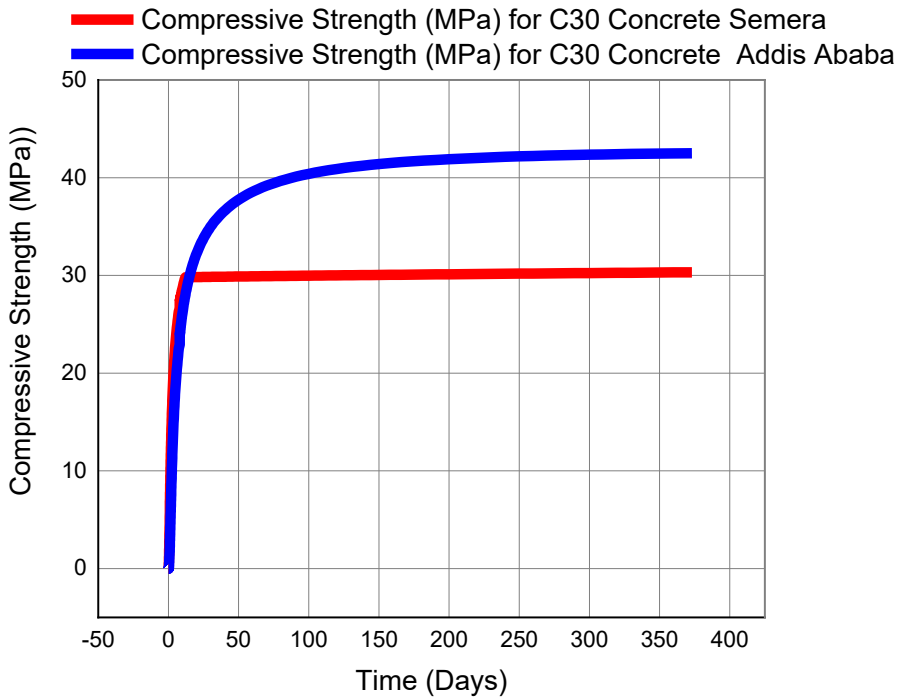

Figure 4-9: Comparison of compressive strength variation with time at different ambient temperatures and relative humidity

4.2 Results of T-girder concrete material under the effect of temperature and relative humidity

To evaluate the effect of volume on drying surface ratio on time-dependent deformation behavior, the same concrete mix at specimen and structure level was investigated.

4.2.1 Results of heat generation

Witnessed in Figure 4-10, the exothermal heat generation is about 42°C for concrete of girder deck whereas for cube specimen with the same mix and at the same environmental conditions, the value is about 38°C. This variation is due to the volume of the drying surface ratio of concrete. From this, it can be noted that when the volume of concrete increases, the exothermic heat generation also increases.

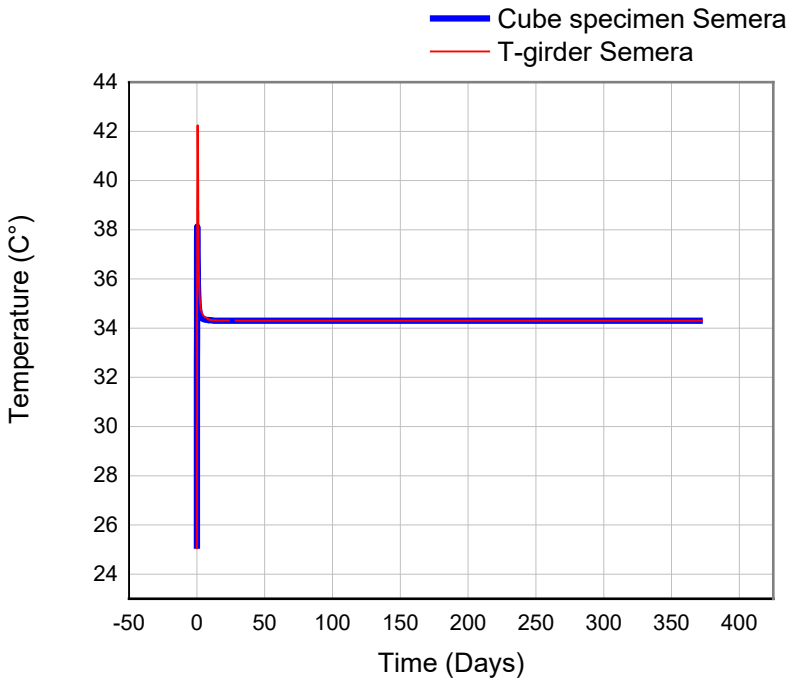

Figure 4-10:Comparison of heat generation at specimen and structure levels at T=34.3°C and RH=47.7%

4.2.2 Results of pores water content

Based on Figure 4-11, at the environment, the amount of water in the pores of the specimen and girder deck level was found nearly the same.

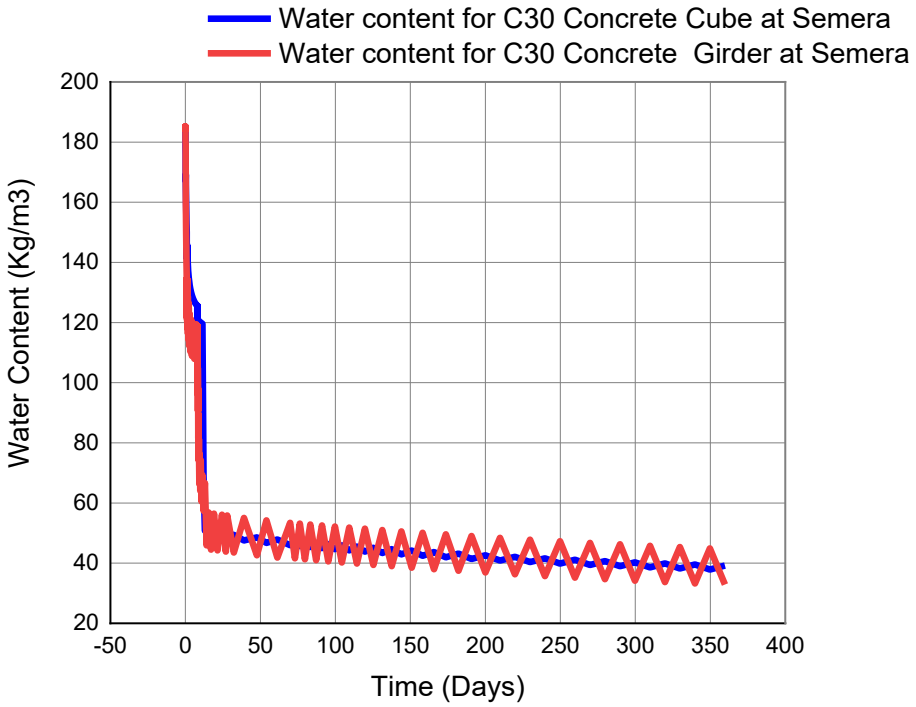

Figure 4-11: Comparison of pores water content at specimen and structure levels at T=34.3°C and RH=47.7%

4.2.3 Results of saturation of interlayer pores

From Figure 4-12, it can be seen that the degree of saturation has a difference at the beginning of the mix at the same environmental condition. The variation became negligible with time. There is a significant variation in the interlayer humidity. As can be seen from Figure 4-13, the interlayer pores humidity of cube specimen is significantly lower than the value of girder with the same material and mix proportion in the same environment. This showed that when the volume of concrete increases the rate and amount of water loss decreases.

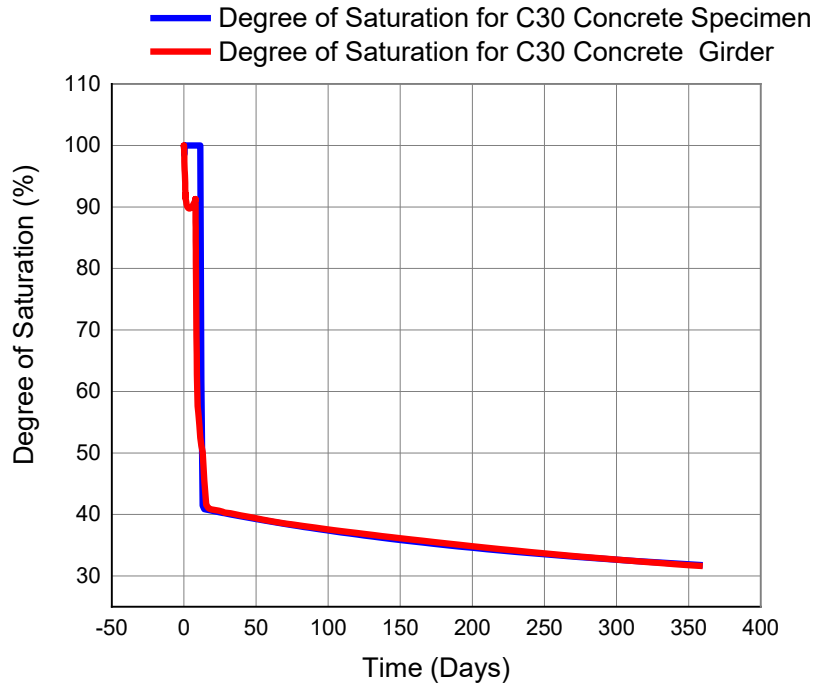

Figure 4-12: Comparison of interlayer pores saturation at specimen and structure levels at T=34.3°C and RH=47.7%

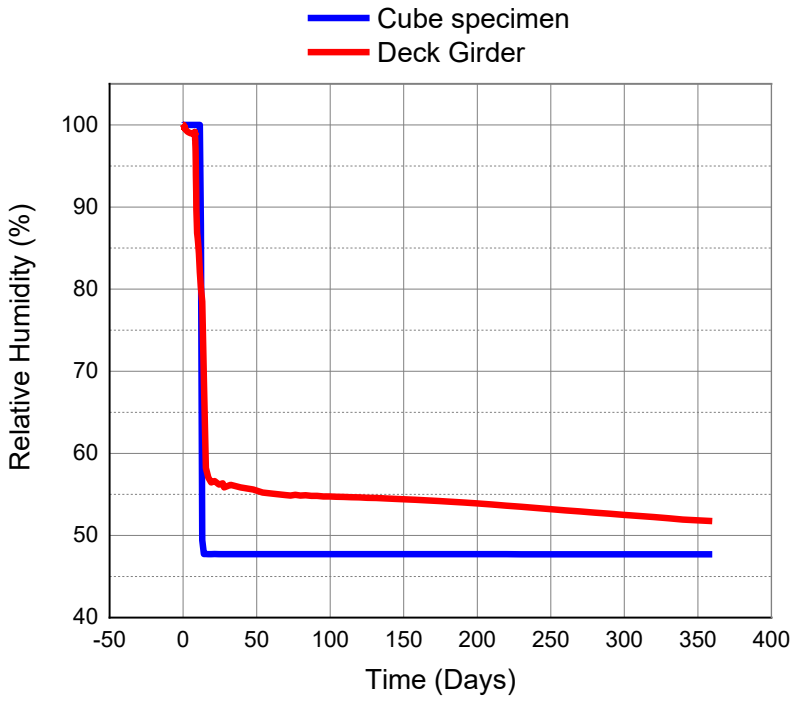

Figure 4-13: Comparison of pores humidity at specimen and structure levels at T=34.3°C and RH=47.7%

4.2.4 Result of the degree of hydration

Figure 4-14 shows there is a significant difference in the value of the degree of hydration at specimen level and structure level. From the figure, it can be noted that when the volume of concrete increases there will be un hydrated cement due to the high heat of generation as shown in Figure 4-10.

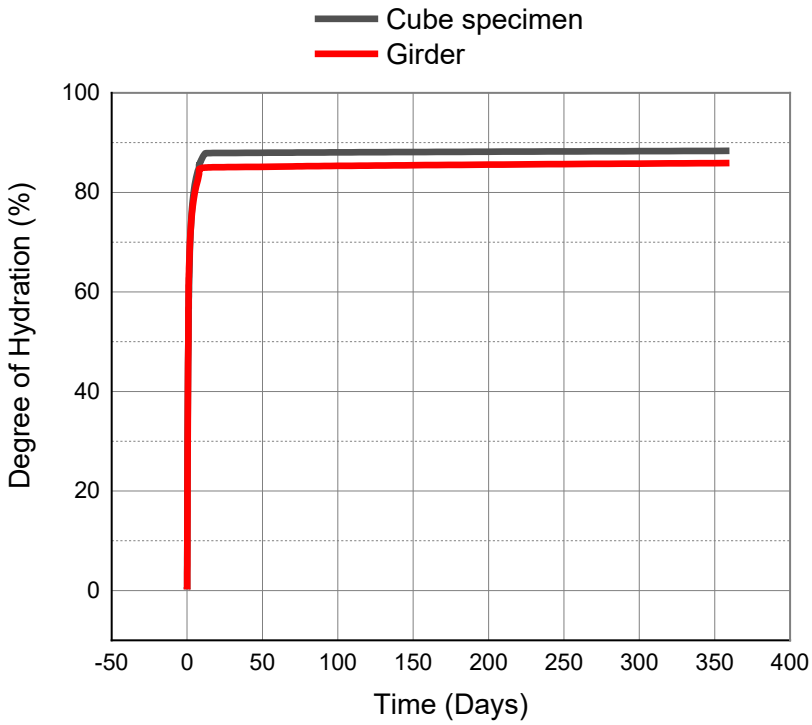

Figure 4-14: Comparison of the degree of hydration at specimen and structure levels at T=34.3°C and RH=47.7%

4.2.5 Result of porosity distribution

Figure 4-15 shows that the porosity distribution is nearly the same at the specimen level and structure level and there is a significant difference in capillary porosity at two levels.

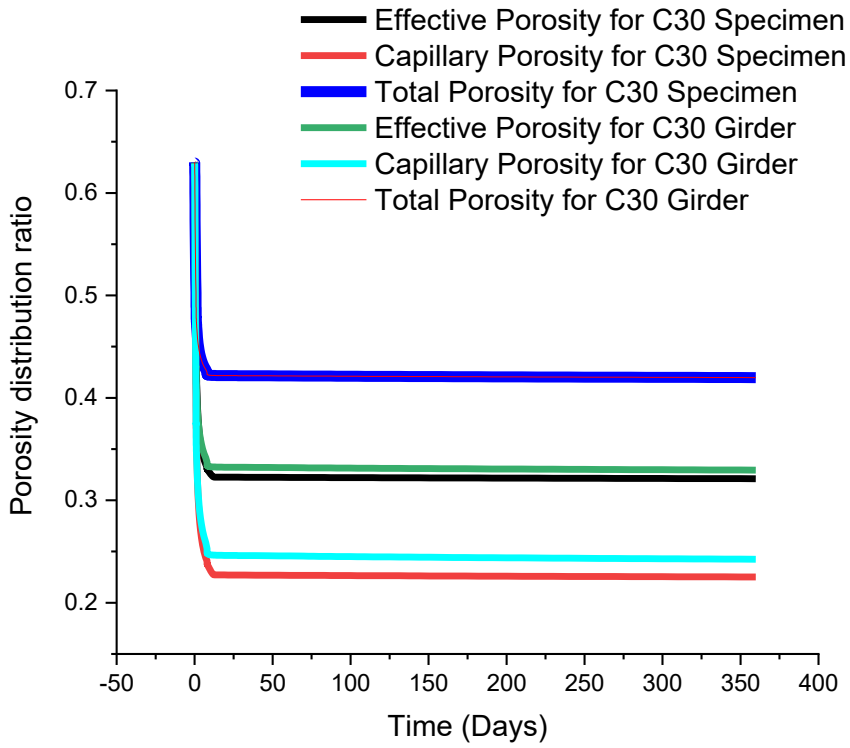

Figure 4-15: Comparison of porosity distribution at specimen and structure levels at T=34.3°C and RH=47.7%

4.2.6 Result of shrinkage strain

Witnessed in Figure 4-16, the shrinkage strain is generally increasing for both conditions with time. The increment is significant at an early age. However, there is a significant difference at specimen and structure level. This is due to interlayer humidity loss as shown in Figure 4-13.

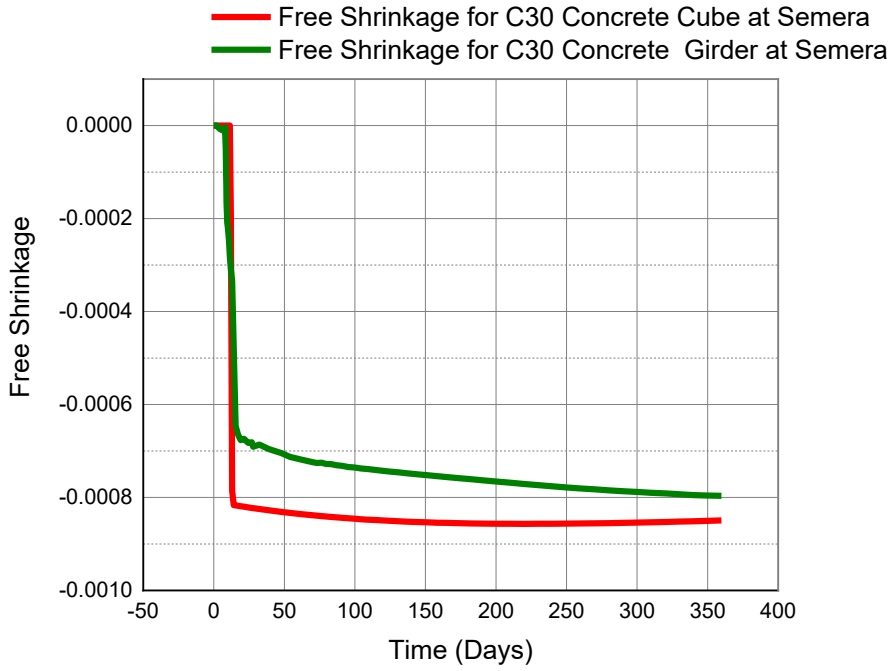

Figure 4-16: Comparison of shrinkage strain at specimen and structure levels at T=34.3°C and RH=47.7%

4.2.7 Result of compressive strength

Due to a lower degree of hydration at the structure level, as shown in Figure 4-14, the strength properties of concrete are decreasing at the structure level. This can be seen from Figure 4-17, that there is a significant difference in compressive strength. The compressive strength obtained at the specimen level is 30.03MPa while, this strength drops to 26.68MPa when cured at the whole structure level. This can be generalized that the strength development in the actual girder is not the same as strength development of specimen of the same material and mix proportion.

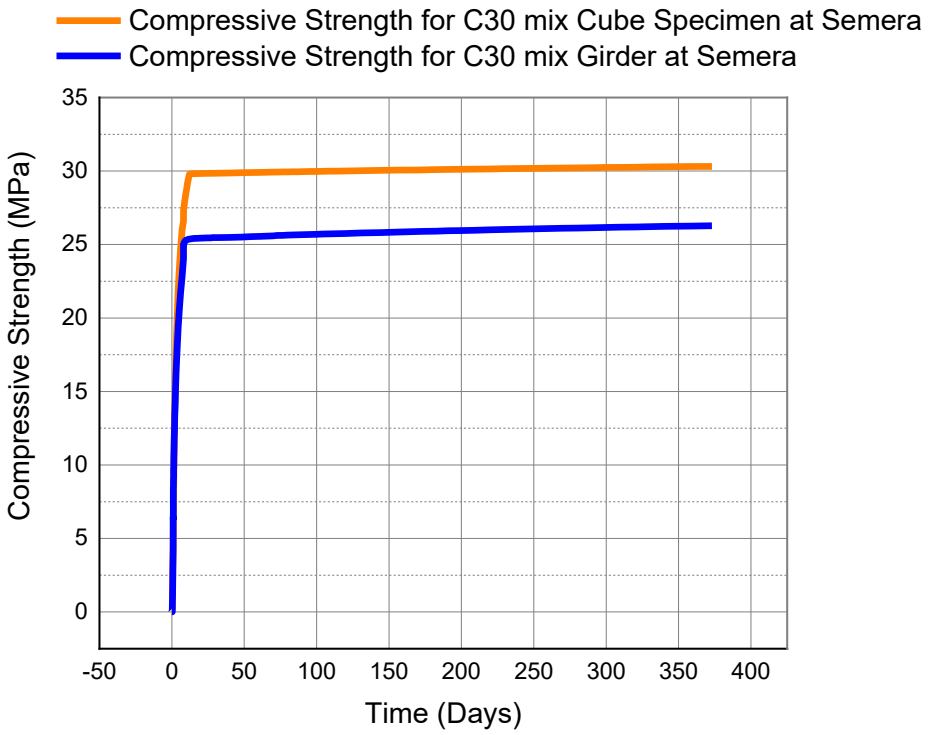

Figure 4-17: Comparison of compressive strength at specimen and structure levels at T=34.3°C and RH=47.7%

4.3 Results of T-girder deck under the effect of temperature and relative humidity

4.3.1 Result of mid-span deflection with time

Girder deck deflection is a commutative effect of early age deformation and delayed plastic deformation. A one-year mid-span deflection obtained based on coupled material-structure analysis that included the effect of temperature and relative humidity was significantly greater than the mid-span deflection of the structure without the effect of ambient temperature and relative humidity. Figure 4-18 has shown that the mid-span deflection based on coupled material-structure analysis including the effect of temperature and relative humidity was nearly 100mm. Whereas this value drops to 25.4mm when the effect of ambient temperature and relative humidity is neglected. This shows that the time-dependent deformation due to the combined effect of applied stress and internal stress by creep and shrinkage is 4 times larger than the deformation due to only applied stress. This is in good agreement with the finding of (Maekawa et al., 2011). A 100mm deflection due

to time-dependent phenomena is more than the design value. The total deflection obtained based on an empirical equation for the design of the girder deck was 87.3mm (APPINDEX-A). This value was underestimated by more than 12% of the actual deflection.

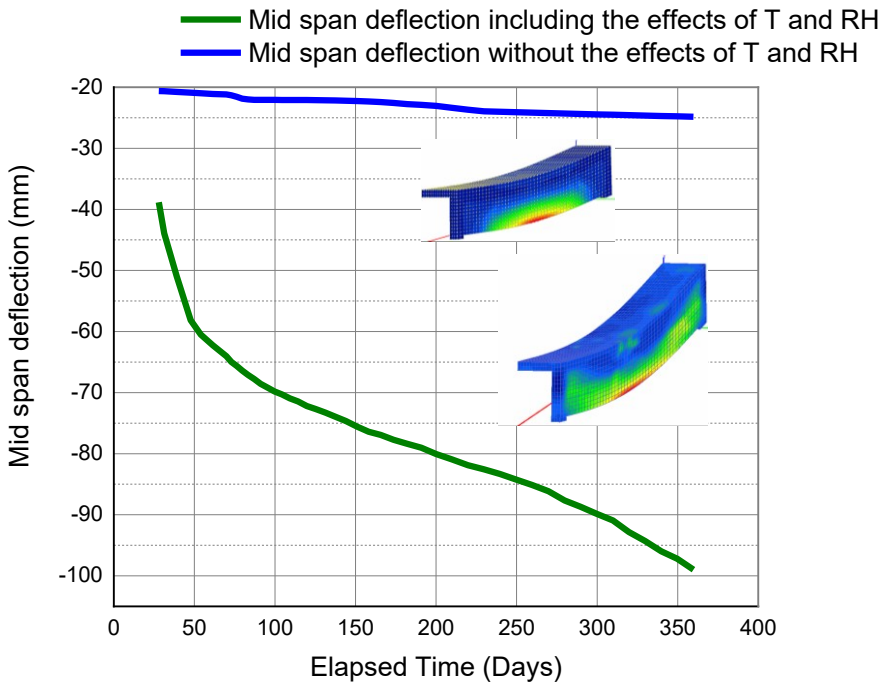

Figure 4-18: Progression of mid-span deflection with time

4.3.2 Result of the rate of creep deformation with time

As shown in Figure 4-19, the rate of deformation with time increases with a decreasing rate. A similar finding was reported in different researches (Gilbert et al., 2010) and (Neville, 1996). And more the 90% of 1-year deformation occurred in 3 months. This shows that after 3 months of construction, there is no significant prestress loss and relaxation or contraction.

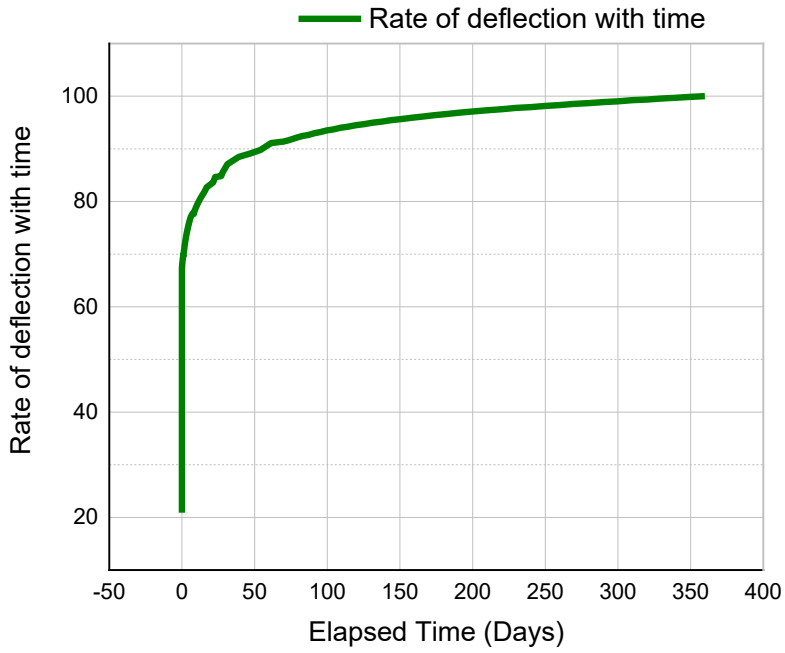

Figure 4-19: Rate of deflection with time

4.3.3 Results of strain progression with time

The graphs in Figure 4-20, has shown that the effect of relative humidity and temperature on the strain progression of reinforced concrete structures. Witnessed in these graphs, the strain development in the concrete due to the effect of the temperature and relative humidity is about double the strain value of the structure without considering the effect of temperature and relative humidity. This strain increase is very significant and it is in good agreement with the results of the findings by (Gilbert et al., 2010) and (Neville, 1996).

As discussed in (Gilbert et al., 2010) and (Neville, 1996) this increment may not have the limit. Based on finding on research by (Neville, 1996), 30 years strain can approximately represent the ultimate value which nearly the same as multiplying the first-year strain by a factor of 1.36. Accordingly, the maximum strain is 0.0012 cm/cm which will be nearly 0.001632 cm/cm after 30 years of service. At 16 years the strain value of 0.00124cm/cm was observed.

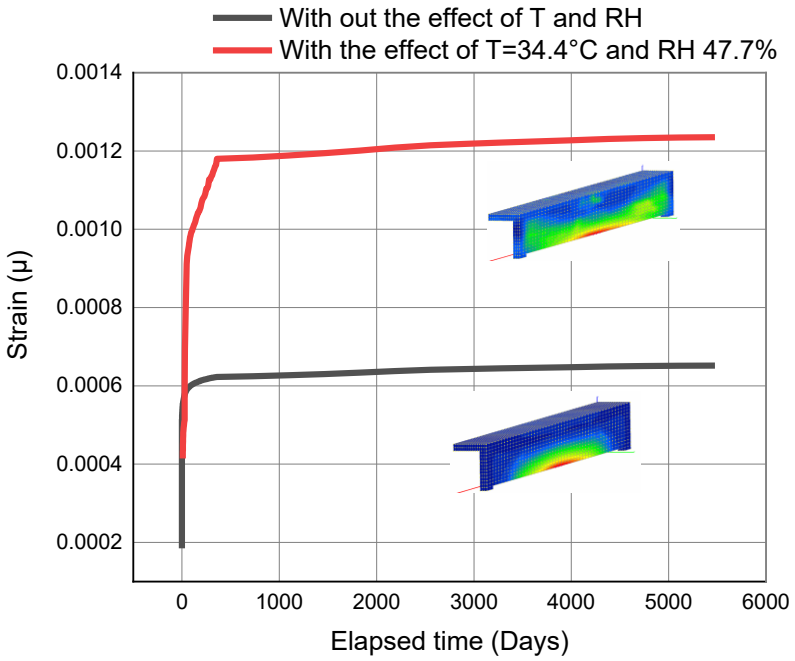

Figure 4-20: Progression of mid-span strain with time

4.3.4 Results of deflection based on contour

The deformation behavior of the structure after analysis and post-processing analysis in the software can be examined using stress contours plots. 1-year deformation contours are presented here for the comparison. From Figure 4-21, it can be noted that the deformation intensity based on coupled material-structure analysis that includes environmental effects is expanding to the support due to micro-pores deformation as water moves from interlayer pores. When the environmental effects are neglected, the intensity of the structure mechanism is in mid-span due to only sustained load.

a) Coupled material-structure analysis (DuCOM-COM3) for 1year 100mm

b) Structural analysis (COM3) for 1-year 25.4mm deflection

Figure 4-21: Comparison of deflection behavior with including and without the effect of temperature and relative humidity

4.3.5 Results of crack formation based on contour

As shown in Figure 4-22, the intensity of the crack formation is significantly different for multi-scale coupled material-structure analysis including the effect of temperature and relative humidity and for structure analysis by neglecting their stresses. There is a significant difference in crack formation after one year of loading (Figure 4-22 e). This is in a good agreement with the finding by different researches (Maekawa et al., 2011), (Asamoto et al., 2006) and (Neville, 1996) that concluded the external environmental factors relative humidity and ambient temperature have a significant effect on the time-dependent properties of concrete.

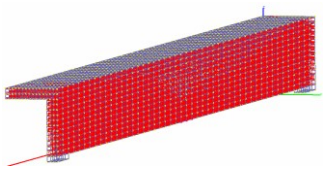

a) Coupled material-structure analysis (DuCOM-COM3) for 3days

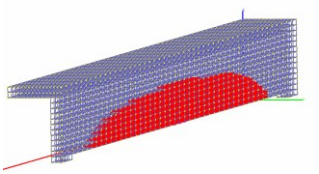

a) Structural analysis (COM3) for 3days

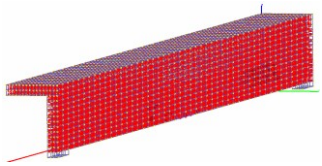

c) Coupled material-structure analysis (DuCOM-COM3) after 1month of loading

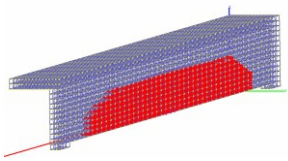

d) Structural analysis (COM3) for after1 month loading of loading

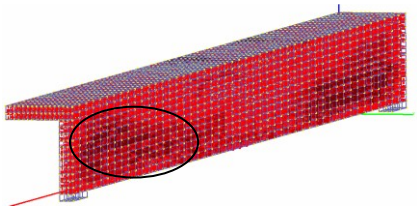

e) Coupled material-structure analysis (DuCOM-COM3) after 1year of loading

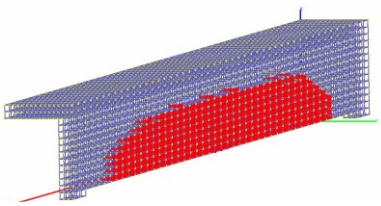

d) Structural analysis (COM3) for after1 month loading of loading

Figure 4-22: Comparison of crack formation with including and without the effect of temperature and relative humidity

CHAPTER 5 CONCLUSIONS AND RECOMMENDATIONS

5.1 Conclusions

In this study, finite element-based time-dependent deformation behavior of the T-girder bridge has been performed on a four T-girder 20m clear span bridge. The analysis was carried out in order to evaluate the time-dependent deformation behavior of reinforced concrete bridge decks due to standard Truckload, lane load and dead load of the structure on the bases of different parameters: nodal reaction-deformation, nodal deformation-time, element stress-time, element strain-time, element principal stress, element principal strain and element reaction-deformation. The current time-dependent analysis finite element model was successfully created in DuCOM-COM3 software. Material modeling including temperature and humidity, geometric modeling, boundary conditions, and loading were accurately treated. The time-dependent analysis by this software successfully captures the deformation behavior of a single-span reinforced concrete T-girder bridge subjected to sustained loading. The results indicate that this software does a good job of predicting the deformation behavior of the reinforced concrete T-girder bridge deck. Based on the investigation result the following observations and conclusion are derived:

1) It is possible to simulate the time-dependent deformation behavior of bridge decks using a time-dependent constitutive model that perform analysis of the micro-pore structure of the concrete and the moisture migration in the micro-pores.
2) Creep deformation increases as the external temperature increases and the relative humidity affect the creep deformation until it reaches an equilibrium state with the external air.
3) In high temperature and low relative humidity environment, the deflection of the bridge deck increases significantly with time and attain an increasing rate with in 3 months accounting more than 90% of 1 year deformation.
4) The deformation of the structure in high temperature and low humidity environment due to the coupled effect of external stress and the internal stresses of creep and shrinkage is about 4 times as large as the deformation due to only applied load.

5) For the environmental conditions with ambient temperature of 34.3°C and relative humidity of 47.7%, the strength property of the specimen has shown significant difference as compared to the strength property of the structure.
6) The deformation is increasing by decreasing rate with time and more than 90% of 1-year deformation could occur within 3 months at the environmental conditions with a temperature of more than 34.3°C and relative humidity less than 47.7%.
7) The over-all result of this investigation has shown that the time-dependent effects of creep and shrinkage should be incorporated in the design of bridges.

5.2 Future research recommendation

The current thesis includes a single-span reinforced concrete T-girder bridge. There is a scope for modeling and analyzing multiple spans or a continuous system. Different parameters like the effect of different girder sizes, girder types, and moving loads need to be further investigated to assess their effects in the reported results. A complete cross-section of a single span bridge consisting of multiple girders can be analyzed. The continuous girder system with the slab and the diaphragm can be modeled to come up with an analysis procedure to find out the actual time-dependent behavior of the bridge system. The current research work can be used as a basis for such analyses. The current study is based on finite element results. In the future, the results from the finite element model can be compared to the bridge monitoring data. Only one material mix proportion is used in this study. However; the effect of aggregate type and size on the creep deformation can be studied. And the effect of cement type and water to cement ratio on creep formation can be investigated. A fixed-point sustained load was used for this study. A more realistic moving load effect on creep can be investigated. The effect of corrosion of reinforcement on the long-term deformation is not considered in the current research. The effect of corrosion of reinforcement in addition to the current study can be investigated. In this study, only material nonlinearity is considered. By considering bridge deck stiffness matrices, the mutual effect of both material and geometric nonlinearity can be investigated.

REFERENCES

ACI Committee 209, ACI. (2008). *Guide for Modeling and Calculating Shrinkage and Creep in Hardened Concrete.*

ACI Committee 211, ACI.(1991). *Standard Practice for Selecting Proportions for Normal, Heavyweight, and Mass Concrete*. *Reapproved*, 1–38.

ACI Committee 231, ACI. (2010). *Report on Early-Age Cracking: Causes, Measurement and Mitigation.*

Asamoto, S., Ishida, T., & Maekawa, K. (2006). Time-dependent constitutive model of solidifying concrete based on thermodynamic state of moisture in fine pores. *Journal of Advanced Concrete Technology*, *4*(2), 301–323.

AASHTO, (2002). Standard Specification for Highway Bridges,17th Edition (2002). American Association of State Highway and Transport Officials; Washington DC (2002).

Baweja, S. (2001). *Creep and Shrinkage Prediction Model for Analysis and Design of Concrete Structures : Model B3 By Zden ˇ. 83*, 38–39.

Bažant, Z. P., Li, G. H., & Yu, Q. (2009). Prediction of creep and shrinkage and their effects in concrete structures: Critical appraisal. *Creep, Shrinkage and Durability Mechanics of Concrete and Concrete Structures - Proceedings of the 8th Int. Conference on Creep, Shrinkage and Durability Mechanics of Concrete and Concrete Structures*, *2*, 1275–1289.

Bažant, Z. P., & Milan, J. (2018). *Creep and Hygrothermal Effects in Concrete Structures*.

Construction Ministry of Ethiopia. (2015). *ES EN 1992:2015 Design of concrete structures - Part 1: General rules and rules for buildings*.

Gilbert, R. I., Engineering, C., Wales, N. S., Australian, C., Fellowships, P., Ranzi, G., Lecturer, S., & Engineering, S. (2010). Time-Dependent Behaviour of Concrete Structures. In *Time-Dependent Behaviour of Concrete Structures*.

Ishida, T., Pen, K., Tanaka, Y., Kashimura, K., & Iwaki, I. (2018). Numerical simulation

of early-age cracking of reinforced concrete bridge decks with a full-3D multiscale and multi-chemo-physical integrated analysis. *Applied Sciences (Switzerland)*, *8*(3).

Maekawa, K., Chijiwa, N., & Gebreyouhannes, E. (2011). *Multi-Scale Simulation of Thermo-Hygro Mechanics on Rc-Pc Structures Under Long-Term Actions*. *December 2015*.

Maekawa, K., Ishida, T., & Kishi, T. (2003). Multi-scale Modeling of Concrete Performance. *Journal of Advanced Concrete Technology*, *1*(2), 91–126.

Min, K., Kwon, K., Kim, Y., Yang, J., & Yoon, Y. (2009). *An experimental study on time-dependent behaviors of early-aged concrete in various curing environments*. 387–393.

Mu, R., Forth, J. P., & Beeby, A. W. (2009). Designing concrete with special shrinkage and creep requirements. *Creep, Shrinkage and Durability Mechanics of Concrete and Concrete Structures - Proceedings of the 8th Int. Conference on Creep, Shrinkage and Durability Mechanics of Concrete and Concrete Structures*, *2*, 1433–1439.

Neville, A. M. (1996). Properties of concrete (fourth edition). In *Cement and Concrete Research* (Vol. 26, Issue 8).

Nomy Engineering PLC. (2015). Analysis and Design Report and working drawings for 20m clear span T-girder Bridge.

Pauw, A. (1971). *Time-dependent deformations of concrete*.

Rüsch, H., Jungwirth, D., & Hilsdorf, H. K. (1983). Creep and Shrinkage. *Creep and Shrinkage*, *December*.

T.Paulay, R. Park. (1975). *Reinforced Concrete Structures*.

Tanaka, H., & Hashida, H. (2009). Effect of limestone as an aggregate on reducing drying shrinkage of concrete. *Creep, Shrinkage and Durability Mechanics of Concrete and Concrete Structures - Proceedings of the 8th Int. Conference on Creep, Shrinkage and Durability Mechanics of Concrete and Concrete Structures*, *2*, 877–883.

Vandamme, M., & Ulm, F. (2009). *Nanogranular origin of concrete creep*. *106*(26), 6–8.

Wittmann, F. H. (2009). Heresies on shrinkage and creep mechanisms. *Creep, Shrinkage and Durability Mechanics of Concrete and Concrete Structures - Proceedings of the 8th Int. Conference on Creep, Shrinkage and Durability Mechanics of Concrete and Concrete Structures*, *1*, 3–9.

Y.Qiang; T.Teng. (n.d.). *Coupled Effects of Static Creep, Cyclic Creep, and Damage on the Long-Term Performance of Prestressed Concrete Bridges: A Case Study Based on Rate-Type Formulation*.

APPENDIX

APPENDIX-A NOMY ENGINEERING PLC. LONG TERM DEFLECTION CALCULATION BASED ON CODE EMPIRICAL FORMULA

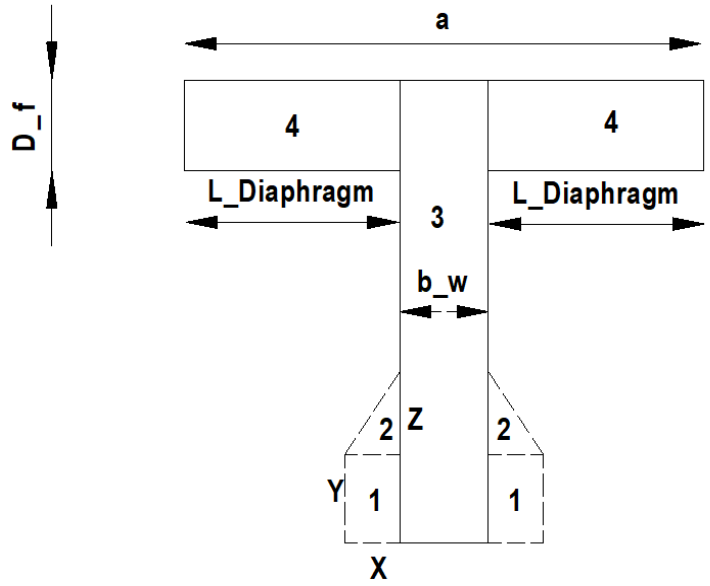

Depth of slab flange, Df=0.22m

Length of the diaphragm, L_D=0.83m

Width of girder web, bw=0.45m

Gross depth of girder including slab=1.45m

X=0

Y=0

Z=0

First Moment of Area

Item	Area (m^2)	Centroid (m)	Area* Centroid (m^3)
1	0.0000	0.0000	0.0000
2	0.0000	0.0000	0.0000
3	0.6525	0.7250	0.4731
4	0.4025	1.3350	0.5373
Total	1.0550		1.0104

$\hat{Y}$ = 0.9577 m

Gross Moment of Inertia

Item	Area (m^2)	Yi (m)	Icg(m^4)	d =$\hat{Y}$ -Yi (m)	Ad²(m^4)	I_tot (m^4)
1	0.0000	0.0000	0.00000	0.9577	0.0000	0.00000
2	0.0000	0.0000	0.00000	0.9577	0.0000	0.00000
3	0.6525	0.7250	0.11432	0.2327	0.0353	0.14966
4	0.4025	1.3350	0.00177	-0.3773	0.0573	0.05906

Gross moment of Inertia Ig = 0.20873 m^4

Ig = 2.09E+11 mm^4

Cracked Section Moment of Inertia

$$k = \frac{n\rho + \frac{1}{2}\left(\frac{D-f}{d}\right)^2}{n\rho + \left(\frac{D-f}{d}\right)}$$

Where:

n =8.00

ρ =0.005697

d=1210.00mm

k =0.2701

Item	Area (m^2)	Yi (m)	Icg(m^4)	d =kd -Yi (m)	Ad^2(m^4)	I_tot (m^4)
Flange	0.50600	0.11500	0.00223	0.21178	0.02269	0.02492
Web	0.04355	0.27839	0.0000339884	0.04839	0.00010	0.00014
Steel	0.11581	1.21000	0.00000	-0.88322	0.09034	0.09034

Icr = 0.11540 m^4

Icr = 1.15E+11 mm^4

$$M_{cr} = f_r \frac{I_g}{y_t}$$

$$f_r = 0.62\sqrt{f_c'}$$

f_r =3.04 N/mm^2

Mcr =1.29E+09Nmm

Ma=M_{max}=3365.83 KNm

$$I_e = \left(\frac{M_{cr}}{M_a}\right)^3 I_g + \left[1 - \left(\frac{M_{cr}}{M_a}\right)^3\right] I_{cr} \le I_g$$

I_e =1.21E+11 mm^4

Since I_e<I_g, section provided is adequate

Dead Load Deflection

$$\Delta_S = \frac{5WL^4}{384EI} + \frac{PL^3}{48EI}$$

Parameter	Value	Unit
The dead load, W	31.11	KN/m
Diaphram weight, P	17.01	KN
Center to center span length	20.50	m
Initial modulus of Elasticity, E	24.77	GPa
Effective area moment of inertia, I_e	1.21E+11	mm^4

Substituting the corresponding values in $\Delta_S = \frac{5WL^4}{384EI} + \frac{PL^3}{48EI}$, one can get the short-term deflection due to dead load $\Delta_S = 0.02621m = 2.621cm$

The long-term deflection can be calculated from the formula based on short term deflection.

$$\Delta_{long} = \Delta_s \left[3 - \frac{1.2As'}{Ast} \right]$$

Where As' = compression reinforcement

Ast = total reinforcement

As'	555.63	mm²
As	14476.46	mm²
Total Ast	15032.08	mm²

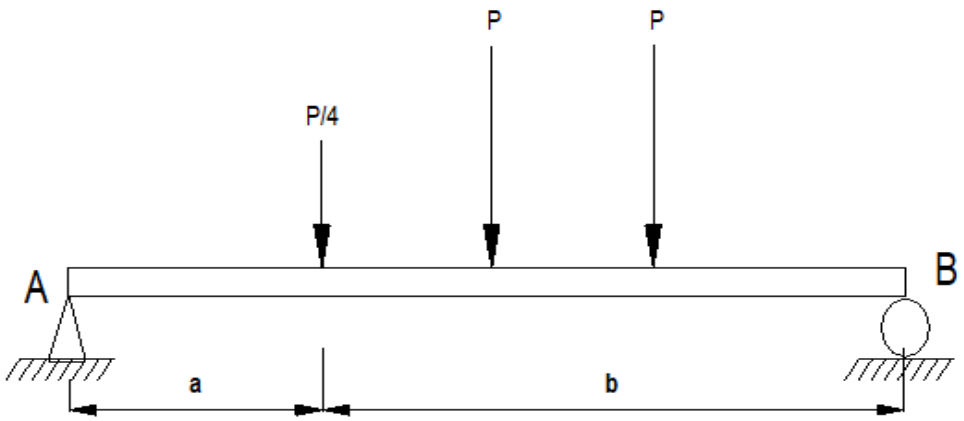

Load	a	b	L/2=X
P/4	4.303	15.697	10.25
P	8.603	11.397	10.25
P	12.903	7.097	10.25

By substituting the corresponding values in $\Delta_{long} = \Delta_s \left[3 - \frac{1.2As'}{Ast} \right]$, the long-term deflection due to total dead load is 7.38cm.

Live Load Deflection

The deflection due to live load is given by the formulas:

Due to $\frac{P}{4}, \Delta_1 = \frac{P}{EI}\left(\frac{-bX^3}{6L} + \frac{(X-a)^3}{6} + \frac{bX(L^2-b^2)}{6L} \right)$

Due to P, at 0.711m shift before Mid-Span, $\Delta_2 = \frac{Pb(L^2-b^2)}{48EI}$

Due to P, after Mid- Span, $\Delta_3 = \frac{Pb(L^2-b^2)}{48EI}$

Due to P/4, $\Delta_1 = 0.00102m$

Due to P, at Mid Span, $\Delta_2 = 0.00457m$

Due to P After Mid-Span, $\Delta_3 = 0.00283m$

Total Live load $\Delta_{total} = 0.00859m$

Distribution factor for wheel loads $= (1+I)x(2-\frac{d}{a})$

d=1.8m lateral spacing of wheels and a = 2.2m center to center spacing of girder

Distribution factor for wheel loads $= (1+0.33)x(2-\frac{1.8}{2.2})$ =1.572

Design total Live Load deflection, Δ_{total} using a distribution factor of 1.572 = 0.0135m

Total LL Deflection =13.5mm

Allowable Live Load Deflection Dall = L/800 =25.625mm.

The total deflection is thus, = 73.8mm+13.5mm=87.3mm

APPENDIX-B LOAD STEPS AND LOAD VALUES DEFINED IN COM3

Step	Time (days)	Acceleration (m/s^2)	Loads (KN)	Step	Time (days)	Acceleration (m/s^2)	Loads
1	0.0002	9.8	0	52	1.0057	9.8	0
2	0.0006	9.8	0	53	1.0066	9.8	0
3	0.0011	9.8	0	54	1.0077	9.8	0
4	0.0016	9.8	0	55	1.009	9.8	0
5	0.0022	9.8	0	56	1.0103	9.8	0
6	0.0025	9.8	0	57	1.0118	9.8	0
7	0.0032	9.8	0	58	1.0134	9.8	0
8	0.0039	9.8	0	59	1.0152	9.8	0
9	0.0048	9.8	0	60	1.0172	9.8	0
10	0.0057	9.8	0	61	1.0194	9.8	0
11	0.0066	9.8	0	62	1.0218	9.8	0
12	0.0077	9.8	0	63	1.0245	9.8	0
13	0.009	9.8	0	64	1.029	9.8	0
14	0.0103	9.8	0	65	1.0342	9.8	0
15	0.0118	9.8	0	66	1.0403	9.8	0
16	0.0134	9.8	0	67	1.0474	9.8	0
17	0.0152	9.8	0	68	1.0555	9.8	0
18	0.0172	9.8	0	69	1.065	9.8	0
19	0.0194	9.8	0	70	1.076	9.8	0
20	0.0218	9.8	0	71	1.0934	9.8	0
21	0.0245	9.8	0	72	1.1146	9.8	0
22	0.029	9.8	0	73	1.1405	9.8	0
23	0.0342	9.8	0	74	1.1719	9.8	0
24	0.0403	9.8	0	75	1.2102	9.8	0
25	0.0474	9.8	0	76	1.2569	9.8	0
26	0.0555	9.8	0	77	1.3137	9.8	0
27	0.065	9.8	0	78	1.3829	9.8	0
28	0.076	9.8	0	79	1.4672	9.8	0
29	0.0934	9.8	0	80	1.5698	9.8	0
30	0.1146	9.8	0	81	1.6948	9.8	0
31	0.1405	9.8	0	82	1.847	9.8	0
32	0.1719	9.8	0	83	2.0324	9.8	0
33	0.2102	9.8	0	84	2.2581	9.8	0
34	0.2569	9.8	0	85	2.533	9.8	0
35	0.3137	9.8	0	86	2.8678	9.8	0
36	0.3829	9.8	0	87	3.2755	9.8	0
37	0.4672	9.8	0	88	3.772	9.8	0

38	0.5698	9.8	0	89	4.3767	9.8	0
39	0.6948	9.8	0	90	5.1131	9.8	0
40	0.847	9.8	0	91	6.0099	9.8	0
41	0.8568	9.8	0	92	7.102	9.8	0
42	1	9.8	0	93	8	9.8	0
43	1.0002	9.8	0	94	8.0002	9.8	0
44	1.0006	9.8	0	95	8.0006	9.8	0
45	1.0011	9.8	0	96	8.0011	9.8	0
46	1.0016	9.8	0	97	8.0016	9.8	0
47	1.0022	9.8	0	98	8.0022	9.8	0
48	1.0025	9.8	0	99	8.0025	9.8	0
49	1.0032	9.8	0	100	8.0032	9.8	0
50	1.0039	9.8	0	101	8.0039	9.8	0
51	1.0048	9.8	0	102	8.0048	9.8	0

Step	Time (days)	Acceleration	Loads	Step	Time (days)		Loads
103	8.0057	9.8	0	158	76.2551	9.8	0
104	8.0066	9.8	0	159	79.7022	9.8	0
105	8.0077	9.8	0	160	83.3234	9.8	0
106	8.009	9.8	0	161	87.1274	9.8	0
107	8.0103	9.8	0	162	91.1235	9.8	0
108	8.0118	9.8	0	163	95.3215	9.8	0
109	8.0134	9.8	0	164	99.7314	9.8	0
110	8.0152	9.8	0	165	104.3641	9.8	0
111	8.0172	9.8	0	166	109.2306	9.8	0
112	8.0194	9.8	0	167	114.343	9.8	0
113	8.0218	9.8	0	168	119.7135	9.8	0
114	8.0245	9.8	0	169	125.3553	9.8	0
115	8.029	9.8	0	170	131.2819	9.8	0
116	8.0342	9.8	0	171	137.5078	9.8	0
117	8.0403	9.8	0	172	144.0482	9.8	0
118	8.0474	9.8	0	173	150.9188	9.8	0
119	8.0555	9.8	0	174	158.1364	9.8	0
120	8.065	9.8	0	175	165.7185	9.8	0
121	8.076	9.8	0	176	173.6835	9.8	0
122	8.0934	9.8	0	177	182.0507	9.8	0
123	8.1146	9.8	0	178	190.8405	9.8	0
124	8.1405	9.8	0	179	200.0742	9.8	0
125	8.1719	9.8	0	180	209.7741	9.8	0
126	8.2102	9.8	0	181	219.7741	9.8	0
127	8.2569	9.8	0	182	229.7741	9.8	0

128	8.3137	9.8	0	183	239.7741	9.8	0
129	8.3829	9.8	0	184	249.7741	9.8	0
130	8.4672	9.8	0	185	259.7741	9.8	0
131	8.5698	9.8	0	186	269.7741	9.8	0
132	8.6948	9.8	0	187	279.7741	9.8	0
133	8.847	9.8	0	188	289.7741	9.8	0
134	9.0324	9.8	0	189	299.7741	9.8	0
135	9.2581	9.8	0	190	309.7741	9.8	0
136	9.533	9.8	0	191	319.7741	9.8	0
137	9.8678	9.8	0	192	329.7741	9.8	0
138	10.2755	9.8	0	193	339.7741	9.8	0
139	10.772	9.8	0	194	349.7741	9.8	0
140	11.3767	9.8	0	195	359.7741	9.8	0
141	12.1131	9.8	0	196	373	9.8	0
142	13.0099	9.8	0	197	374	9.8	0
143	14.102	9.8	0	198	730	9.8	0
144	15.432	9.8	0	199	1095	9.8	0
145	17.0517	9.8	0	200	1460	9.8	0
146	19.5812	9.8	0	201	1825	9.8	0
147	21.4265	9.8	0	202	2190	9.8	0
148	22.8172	9.8	0	203	2555	9.8	0
149	26.9571	9.8	0	204	2920	9.8	0
150	27.9146	9.8	P=36.25,P=36.25, P/4=9.062	205	3285	9.8	0
151	31.2534	9.8	P=36.25,P=36.25, P/4=9.062	206	3650	9.8	0
152	39.029	9.8	P=36.25,P=36.25, P/4=9.024	207	4015	9.8	0
153	47.6972	9.8	P=36.25,P=36.25, P/4=9.024	208	4380	9.8	0
154	54.0208	9.8	0	209	4745	9.8	0
155	61.3517	9.8	0	210	5110	9.8	0
156	69.8501	9.8	0	211	5475	9.8	0
157	72.9737	9.8	0	212	5840	9.8	0